enzymatic activity was determined, in triplicate, by exchange reaction between carbon dioxide and glycine using $NaH^{14}CO_3$ in the presence of excess recombinant bovine GCSH protein as described (22). An expression system of lipoylated bovine GCSH protein in *Escherichia coli* was kindly provided by Dr Kazuko Fujiwara (Tokushima University, Japan) (46). Statistical analysis was performed using SPSS software version 11.0 (SPSS, Inc., Chicago, IL, USA).

Knockout of Amt by insertion of a gene-trap vector

Mice carrying a gene-trap allele of *Amt* (here denoted Amt^{-}) were generated at Lexicon Genetics, Inc. (Houston, TX, USA) using the OST181110 ES cell line. The genomic insertion site of the gene-trap vector was determined by inverse PCR and localized to intron 2 (Supplementary Material, Fig. S1). Total RNA was prepared from the mouse liver and brain at E18 for RT-PCR analysis (Supplementary Material, Fig. S1 and Table S1). $Amt^{+/-}$ mice were backcrossed with wild-type C57BL/6 mice for nine generations to generate a congenic line of mice on the C57BL/6 background, for use in biochemical and histological analyses. This study was approved by the Animal Experiment Committee of Tohoku University.

Maternal supplementation with folic acid and related metabolites

Dams were treated with folic acid (25 mg/kg), thymidine-1-phosphate (TMP; 30 mg/kg) or L-methionine (70 mg/kg) by intra-peritoneal injection, 2 h prior to mating and daily from E7.5–10.5. Doses were based on previous studies (23,47,48).

SUPPLEMENTARY MATERIAL

Supplementary Material is available at *HMG* online.

Conflict of Interest statement. None declared.

FUNDING

This work was supported by a research grant from the Ministry of Education, Culture, Sports, Science and Technology and a Research Grant from the Ministry of Health, Labour and Public Welfare in Japan. Research at Newcastle University was funded by the Newlife Foundation. Research at UCL Institute of Child Health was supported by SPARKS, the Wellcome Trust, Medical Research Council, UCL Biomedical Research Centre and by Great Ormond Street Hospital Children's Charity. Funding to pay the Open Access publication charges for this article was provided by the Wellcome Trust.

REFERENCES

1. Greene, N.D. and Copp, A.J. (2009) Development of the vertebrate central nervous system: formation of the neural tube. *Prenatal Diag.*, **29**, 303–311.
2. Harris, M.J. and Juriloff, D.M. (2007) Mouse mutants with neural tube closure defects and their role in understanding human neural tube defects. *Birth Defects Res. A Clin. Mol. Teratol.*, **79**, 187–210.
3. Greene, N.D.E., Stanier, P. and Copp, A.J. (2009) Genetics of human neural tube defects. *Hum. Mol. Genet.*, **18**, R113–R129.
4. Au, K.S., Ashley-Koch, A. and Northrup, H. (2010) Epidemiologic and genetic aspects of spina bifida and other neural tube defects. *Dev. Disabil. Res. Rev.*, **16**, 6–15.
5. Harris, M.J. and Juriloff, D.M. (2010) An update to the list of mouse mutants with neural tube closure defects and advances toward a complete genetic perspective of neural tube closure. *Birth Defects Res. A Clin. Mol. Teratol.*, **88**, 653–669.
6. Copp, A.J. and Greene, N.D.E. (2010) Genetics and development of neural tube defects. *J. Pathol.*, **220**, 217–230.
7. Blom, H.J., Shaw, G.M., Den Heijer, M. and Finnell, R.H. (2006) Neural tube defects and folate: case far from closed. *Nat. Rev. Neurosci.*, **7**, 724–731.
8. Molloy, A.M., Brody, L.C., Mills, J.L., Scott, J.M. and Kirke, P.N. (2009) The search for genetic polymorphisms in the homocysteine/folate pathway that contribute to the etiology of human neural tube defects. *Birth Defects Res. A Clin. Mol. Teratol.*, **85**, 285–294.
9. Beaudin, A.E. and Stover, P.J. (2009) Insights into metabolic mechanisms underlying folate-responsive neural tube defects: a mini review. *Birth Defects Res. A Clin. Mol. Teratol.*, **85**, 274–284.
10. Tibbetts, A.S. and Appling, D.R. (2010) Compartmentalization of mammalian folate-mediated one-carbon metabolism. *Annu. Rev. Nutr.*, **30**, 57–81.
11. Boyles, A.L., Hammock, P. and Speer, M.C. (2005) Candidate gene analysis in human neural tube defects. *Am. J. Med. Genet. C Semin. Med. Genet.*, **135**, 9–23.
12. Shaw, G.M., Lu, W., Zhu, H., Yang, W., Briggs, F.B., Carmichael, S.L., Barcellos, L.F., Lammer, E.J. and Finnell, R.H. (2009) 118 SNPs of folate-related genes and risks of spina bifida and conotruncal heart defects. *BMC Med. Genet.*, **10**, 49.
13. Martinez, C.A., Northrup, H., Lin, J.I., Morrison, A.C., Fletcher, J.M., Tyerman, G.H. and Au, K.S. (2009) Genetic association study of putative functional single nucleotide polymorphisms of genes in folate metabolism and spina bifida. *Am. J. Obstet. Gynecol.*, **201**, 394–411.
14. Dunlevy, L.P.E., Chitty, L.S., Doudney, K., Burren, K.A., Stojilkovic-Mikic, T., Stanier, P., Scott, R., Copp, A.J. and Greene, N.D.E. (2007) Abnormal folate metabolism in foetuses affected by neural tube defects. *Brain*, **130**, 1043–1049.
15. Parle-McDermott, A., Pangilinan, F., O'Brien, K.K., Mills, J.L., Magee, A.M., Troendle, J., Sutton, M., Scott, J.M., Kirke, P.N., Molloy, A.M. and Brody, L.C. (2009) A common variant in MTHFD1L is associated with neural tube defects and mRNA splicing efficiency. *Hum. Mutat.*, **30**, 1650–1656.
16. Kikuchi, G. (1973) The glycine cleavage system: composition, reaction mechanism, and physiological significance. *Mol. Cell. Biochem.*, **1**, 169–187.
17. Kure, S., Tada, K. and Narisawa, K. (1997) Nonketotic hyperglycinemia: biochemical, molecular, and neurological aspects. *Jpn J. Hum. Genet.*, **42**, 13–22.
18. Kure, S., Narisawa, K. and Tada, K. (1992) Enzymatic diagnosis of nonketotic hyperglycinemia with lymphoblasts. *J. Pediatr.*, **120**, 95–98.
19. Hayasaka, K., Tada, K., Kikuchi, G., Winter, S. and Nyhan, W.L. (1983) Nonketotic hyperglycinemia: two patients with primary defects of P-protein and T-protein, respectively, in the glycine cleavage system. *Pediatr. Res.*, **17**, 967–970.
20. Ichinohe, A., Kure, S., Mikawa, S., Ueki, T., Kojima, K., Fujiwara, K., Iinuma, K., Matsubara, Y. and Sato, K. (2004) Glycine cleavage system in neurogenic regions. *Eur. J. Neurosci.*, **19**, 2365–2370.
21. Toone, J.R., Applegarth, D.A., Kure, S., Coulter-Mackie, M.B., Sazegar, P., Kojima, K. and Ichinohe, A. (2002) Novel mutations in the P-protein (glycine decarboxylase) gene in patients with glycine encephalopathy (non-ketotic hyperglycinemia). *Mol. Genet. Metab.*, **76**, 243–249.
22. Sakata, Y., Owada, Y., Sato, K., Kojima, K., Hisanaga, K., Shinka, T., Suzuki, Y., Aoki, Y., Satoh, J., Kondo, H. *et al.* (2001) Structure and expression of the glycine cleavage system in rat central nervous system. *Brain Res. Mol. Brain Res.*, **94**, 119–130.
23. Fleming, A. and Copp, A.J. (1998) Embryonic folate metabolism and mouse neural tube defects. *Science*, **280**, 2107–2109.

24. Applegarth, D.A., Toone, J.R. and Lowry, R.B. (2000) Incidence of inborn errors of metabolism in British Columbia, 1969–1996. *Pediatrics*, **105**, e10.
25. Nyhan, W.L. (1989) Nonketotic hyperglycinemia. In Scriver, C.R., Beaudet, A.L., Sly, W.S. and Valle, D. (eds), *The Metabolic Basis of Inherited Disease*. McGraw-Hill, Inc., New York, 743–753.
26. Kure, S., Kato, K., Dinopoulos, A., Gail, C., DeGrauw, T.J., Christodoulou, J., Bzduch, V., Kalmanchey, R., Fekete, G., Trojovsky, A. *et al.* (2006) Comprehensive mutation analysis of GLDC, AMT, and GCSH in nonketotic hyperglycinemia. *Hum. Mutat.*, **27**, 343–352.
27. Harris, M.J. (2008) Insights into prevention of human neural tube defects by folic acid arising from consideration of mouse mutants. *Birth Defects Res. A Clin. Mol. Teratol.*, **85**, 331–339.
28. Watanabe, M., Osada, J., Aratani, Y., Kluckman, K., Reddick, R., Malinow, M.R. and Maeda, N. (1995) Mice deficient in cystathionine β-synthase: animal models for mild and severe homocyst(e)inemia. *Proc. Natl Acad. Sci. USA*, **92**, 1585–1589.
29. Champion, K.M., Cook, R.J., Tollaksen, S.L. and Giometti, C.S. (1994) Identification of a heritable deficiency of the folate-dependent enzyme 10-formyltetrahydrofolate dehydrogenase in mice. *Proc. Natl Acad. Sci. USA*, **91**, 11338–11342.
30. Chen, Z., Karaplis, A.C., Ackerman, S.L., Pogribny, I.P., Melnyk, S., Lussier-Cacan, S., Chen, M.F., Pai, A., John, S.W., Smith, R.S. *et al.* (2001) Mice deficient in methylenetetrahydrofolate reductase exhibit hyperhomocysteinemia and decreased methylation capacity, with neuropathology and aortic lipid deposition. *Hum. Mol. Genet.*, **10**, 433–443.
31. MacFarlane, A.J., Liu, X., Perry, C.A., Flodby, P., Allen, R.H., Stabler, S.P. and Stover, P.J. (2008) Cytoplasmic serine hydroxymethyltransferase regulates the metabolic partitioning of methylenetetrahydrofolate but is not essential in mice. *J. Biol. Chem.*, **283**, 25846–25853.
32. Di, P.E., Sirois, J., Tremblay, M.L. and Mackenzie, R.E. (2002) Mitochondrial NAD-dependent methylenetetrahydrofolate dehydrogenase-methenyltetrahydrofolate cyclohydrolase is essential for embryonic development. *Mol. Cell. Biol.*, **22**, 4158–4166.
33. Swanson, D.A., Liu, M.L., Baker, P.J., Garrett, L., Stitzel, M., Wu, J.M., Harris, M., Banerjee, R., Shane, B. and Brody, L.C. (2001) Targeted disruption of the methionine synthase gene in mice. *Mol. Cell. Biol.*, **21**, 1058–1065.
34. Elmore, C.L., Wu, X., Leclerc, D., Watson, E.D., Bottiglieri, T., Krupenko, N.I., Krupenko, S.A., Cross, J.C., Rozen, R., Gravel, R.A. and Matthews, R.G. (2007) Metabolic derangement of methionine and folate metabolism in mice deficient in methionine synthase reductase. *Mol. Genet. Metab.*, **91**, 85–97.
35. Field, M.S., Anderson, D.D. and Stover, P.J. Mthfs is an essential gene in mice and a component of the purinosome. *Front. Genet.* http://www.frontiersin.org/nutrigenomics/10.3389/fgene.2011.00036/abstract.
36. Spiegelstein, O., Mitchell, L.E., Merriweather, M.Y., Wicker, N.J., Zhang, Q., Lammer, E.J. and Finnell, R.H. (2004) Embryonic development of folate binding protein-1 (Folbp1) knockout mice: effects of the chemical form, dose, and timing of maternal folate supplementation. *Dev. Dyn.*, **231**, 221–231.
37. Burren, K.A., Savery, D., Massa, V., Kok, R.M., Scott, J.M., Blom, H.J., Copp, A.J. and Greene, N.D.E. (2008) Gene-environment interactions in the causation of neural tube defects: folate deficiency increases susceptibility conferred by loss of *Pax3* function. *Hum. Mol. Genet.*, **17**, 3675–3685.
38. Beaudin, A.E., Abarinov, E.V., Noden, D.M., Perry, C.A., Chu, S., Stabler, S.P., Allen, R.H. and Stover, P.J. (2011) Shmt1 and de novo thymidylate biosynthesis underlie folate-responsive neural tube defects in mice. *Am. J. Clin. Nutr.*, **93**, 789–798.
39. Nijhout, H.F., Reed, M.C., Lam, S.L., Shane, B., Gregory, J.F. III and Ulrich, C.M. (2006) In silico experimentation with a model of hepatic mitochondrial folate metabolism. *Theor. Biol. Med. Model.*, **3**, 40.
40. Pike, S.T., Rajendra, R., Artzt, K. and Appling, D.R. (2010) Mitochondrial C1-tetrahydrofolate synthase (MTHFD1L) supports the flow of mitochondrial one-carbon units into the methyl cycle in embryos. *J. Biol. Chem.*, **285**, 4612–4620.
41. Dunlevy, L.P.E., Burren, K.A., Mills, K., Chitty, L.S., Copp, A.J. and Greene, N.D.E. (2006) Integrity of the methylation cycle is essential for mammalian neural tube closure. *Birth Defects Res. A*, **76**, 544–552.
42. Greene, N.D., Stanier, P. and Moore, G.E. (2011) The emerging role of epigenetic mechanisms in the actiology of neural tube defects. *Epigenetics*, **6**, 875–893.
43. Apostolidou, S., Abu-Amero, S., O'Donoghue, K., Frost, J., Olafsdottir, O., Chavele, K.M., Whittaker, J.C., Loughna, P., Stanier, P. and Moore, G.E. (2007) Elevated placental expression of the imprinted PHLDA2 gene is associated with low birth weight. *J. Mol. Med.*, **85**, 379–387.
44. Niwa, H., Yamamura, K. and Miyazaki, J. (1991) Efficient selection for high-expression transfectants with a novel eukaryotic vector. *Gene*, **108**, 193–199.
45. Oda, M., Kure, S., Sugawara, T., Yamaguchi, S., Kojima, K., Shinka, T., Sato, K., Narisawa, A., Aoki, Y., Matsubara, Y. *et al.* (2007) Direct correlation between ischemic injury and extracellular glycine concentration in mice with genetically altered activities of the glycine cleavage multienzyme system. *Stroke*, **38**, 2157–2164.
46. Fujiwara, K., Okamura-Ikeda, K. and Motokawa, Y. (1991) Lipoylation of H-protein of the glycine cleavage system. The effect of site-directed mutagenesis of amino acid residues around the lipoyllysine residue on the lipoate attachment. *FEBS Lett.*, **293**, 115–118.
47. Wlodarczyk, B.J., Tang, L.S., Triplett, A., Aleman, F. and Finnell, R.H. (2006) Spontaneous neural tube defects in splotch mice supplemented with selected micronutrients. *Toxicol. Appl. Pharmacol.*, **213**, 55–63.
48. Essien, F.B. and Wannberg, S.L. (1993) Methionine but not folinic acid or vitamin B-12 alters the frequency of neural tube defects in *Axd* mutant mice. *J. Nutr.*, **123**, 27–34.
49. Nakai, T., Nakagawa, N., Maoka, N., Masui, R., Kuramitsu, S. and Kamiya, N. (2005) Structure of P-protein of the glycine cleavage system: implications for nonketotic hyperglycinemia. *EMBO J.*, **24**, 1523–1536.

Journal of the Neurological Sciences 315 (2012) 77–81

Contents lists available at SciVerse ScienceDirect

Journal of the Neurological Sciences

journal homepage: www.elsevier.com/locate/jns

Hypoperfusion in caudate nuclei in patients with brain–lung–thyroid syndrome

Mitsugu Uematsu [a,*], Kazuhiro Haginoya [b], Atsuo Kikuchi [a], Tojo Nakayama [a], Yousuke Kakisaka [a], Yurika Numata [a], Tomoko Kobayashi [a], Naomi Hino-Fukuyo [a], Ikuma Fujiwara [a], Shigeo Kure [a]

[a] Department of Pediatrics, Tohoku University School of Medicine, Sendai, Japan
[b] Department of Pediatric Neurology, Takuto Rehabilitation Center for Children, Sendai, Japan

ARTICLE INFO

Article history:
Received 20 August 2011
Received in revised form 11 November 2011
Accepted 15 November 2011
Available online 12 December 2011

Keywords:
Brain–lung–thyroid syndrome
NKX2-1
Array CGH
ECD-SPECT
eZIS

ABSTRACT

Mutations in *NKX2-1* cause neurological, pulmonary, and thyroid hormone impairment. Recently, the disease was named brain–lung–thyroid syndrome. Here, we report three patients with brain–lung–thyroid syndrome. All patients were unable to walk until 24 months of age, and still have a staggering gait, without mental retardation. They have also had choreoathetosis since early infancy. Genetic analysis of *NKX2-1* revealed a novel missense mutation (p.Val205Phe) in two patients who were cousins and their maternal families, and a novel 2.6-Mb deletion including *NKX2-1* on chromosome 14 in the other patient. Congenital hypothyroidism was not detected on neonatal screening in the patient with the missense mutation, and frequent respiratory infections were observed in the patient with the deletion in *NKX2-1*. Oral levodopa did not improve the gait disturbance or involuntary movement. The results of ^{99m}Tc-ECD single-photon emission computed tomography (ECD-SPECT) analyzed using the easy Z-score imaging system showed decreased cerebral blood flow in the bilateral basal ganglia, especially in the caudate nuclei, in all three patients, but no brain magnetic resonance imaging (MRI) abnormalities. These brain nuclear image findings indicate that *NKX2-1* haploinsufficiency causes dysfunction of the basal ganglia, especially the caudate nuclei, resulting in choreoathetosis and gait disturbance in this disease.

1. Introduction

NK2 homeobox 1 (*NKX2-1* or *TITF-1*; MIM #600635), which maps on chromosome 14q13, is a member of the *NK-2* gene family of highly conserved homeodomain-containing transcription factors [1,2]. The gene is expressed in the thyroid, bronchial epithelium, and specific areas of the forebrain during development in the mouse [3–5]. Mice homozygous for the disrupted gene are born dead and lack a thyroid gland, lung parenchyma, and pituitary gland, while heterozygous mice develop normally [4]. An abnormality of the gene in humans was first reported in patients with congenital hypothyroidism [6]. Subsequently, heterozygous point mutations in *NKX2-1* were identified in affected members of a family with benign hereditary chorea [7]. Recently, *NKX2-1* was reported as the gene responsible for brain–lung–thyroid syndrome (MIM #610978), which involves symptoms of neurological impairment, pulmonary disorders, and hypothyroidism [8–13]. Respiratory distress during the neonatal period, recurrent respiratory tract infection, and hypothyroidism are common clinical findings. The neurological impairment is characterized by gait disturbance with delayed first walking and choreoathetosis, in the absence of mental retardation or brain magnetic resonance imaging (MRI) abnormalities [13]. However, some affected individuals have had low-average intelligence, learning problems, psychosis and seizures [14–16].

The pathological mechanism of *NKX2-1* haploinsufficiency has been clarified for the hypothyroidism [17] and pulmonary impairment [18,19], but it is still unclear for the neurological symptoms. Most of the neurological deficits, i.e., the gait disturbance and involuntary movements sometimes accompanied with dystonia, dysarthria, action tremor and saccadic abnormalities [20], reflect dysfunction of the control of movement. Therefore, the basal ganglia were considered to be the most important causal lesion [8,14]. The *NKX2-1* null mouse showed severe morphological changes in the basal ganglia, including absence of the globus pallidus and enlargement of the striatum [4]. *NKX2-1* gene expression has been identified as the origin of the pallidum in the mammalian and avian embryonic archistriatum. These studies indicated that *NKX2*-1 is essential for development of the striatum, especially the pallidum rather than the caudate nuclei [5,21,22].

Brain MRI of patients with brain–lung–thyroid syndrome showed no notable abnormalities, except one case report of reduced size and intensity in the pallidum [8]. Previous brain nuclear imaging studies described various findings regarding the basal ganglia, including reduced blood flow in the striatum and thalamus [23], and hypometabolism in the basal ganglia, more prominent in the caudate nuclei [15].

* Corresponding author at: Department of Pediatrics, Tohoku University School of Medicine, 1-1 Seiryo-machi, Aoba-ku, Sendai 980-8574, Japan. Tel: +81 22 717 7287; fax: +81 22 717 7290.
E-mail address: uematsu@bk9.so-net.ne.jp (M. Uematsu).

0022-510X/$ – see front matter © 2011 Elsevier B.V. All rights reserved.
doi:10.1016/j.jns.2011.11.025

Here, we report three patients with brain–lung–thyroid syndrome in whom the diagnosis was confirmed by genetic examinations. We performed brain nuclear image analysis to investigate the causal lesion for the neurological symptoms.

2. Method

2.1. Clinical findings

We studied three patients (5, 6, and 7 years old; one male and two females) with gait disturbance who visited Tohoku University Hospital between 2008 and 2009 (Table 1).

Patient 1 was the second female child of healthy non-consanguineous parents (Fig. 1). She was born at term without neonatal respiratory problems. Congenital hypothyroidism was noted on neonatal screening and she has been given thyroxin replacement therapy since then. After the age of 1.6 years, she developed recurrent respiratory infections and was admitted to hospital five times in one year. She had normal mental development, but delayed gross motor development. She could sit alone at the age of 12 months and first walked at 38 months. A staggering gait persists. Her trunk and extremes were mildly hypotonic and continuous choreoathetosis was observed during wakefulness and exacerbated by stress.

Patients 2 and 3 were cousins via their maternal families (Fig. 1). Patient 2 was the third female and Patient 3 was an only male child. Both sets of non-consanguineous parents were healthy fathers and affected mothers with mild involuntary movement and a history of delayed first walking. Both patients were born at term without any perinatal complications. Congenital hypothyroidism was diagnosed in the neonatal period by screening in Patient 2, but at the age of 5 years in Patient 3, despite a neonatal screening test. Unlike Patient 1, they had no severe respiratory infections during infancy. Similar to Patient 1, first walking was observed at 30 months in Patient 2 and at 24 months in Patient 3. They also have persistent gait disturbance and choreoathetosis without mental retardation. The neurological examinations in all three patients did not detect any abnormalities, such as muscle weakness, abnormal deep tendon reflexes, or cerebellar manifestations.

Brain MRI in all three patients showed normal brain size, form, and intensity, including the basal ganglia. Oral levodopa (20 mg/kg/day) was given to all three patients, but no obvious improvement in the neurological symptoms was observed.

2.2. Brain nuclear image analysis

All three patients underwent single photon emission computed tomography (SPECT) to evaluate brain function at Tohoku University Hospital using technetium-99 m ethyl cysteinate dimer (ECD,

Table 1
Clinical characteristics in three patients.

	Patient 1	Patient 2	Patient 3
Age/sex	7 years/female	5 years/female	6 years/male
Recurrence of respiratory infection	Yes	No	No
Neonatal respiratory problems	No	No	No
Hypothyroidism	Yes (neonatal screening)	Yes (neonatal screening)	Yes (diagnosed at 5 years)
Initiation of walking	3 years and 2 months	2 years and 6 months	2 years
Mental retardation	No	No	No
Choreoathetosis	Yes	Yes	Yes
Response to L-dopa	No	No	No
Brain MRI	Normal	Normal	Normal
NKX2-1 analysis	del 14q12–13	p.V205P	p.V205P

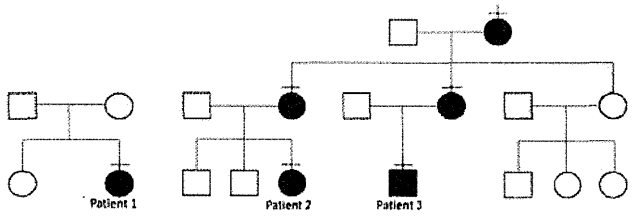

Fig. 1. Family pedigrees of three patients. Affected members are indicated by black squares and circles; unaffected members, white squares and circles. Patient 2 and 3 are cousins on mother's side.

approximately 12 MBq/kg of body weight) as the radiotracer. Twenty minutes after the injection, SPECT images were acquired using a PRISM IRIX (Shimadzu, Kyoto, Japan), with a low-energy, high-resolution, fan-beam collimator. In total, 120 projection datum points in a 128×128 matrix were obtained in 20 min. Using an ODYSSEY computer (Shimadzu), tomograms two pixels thick (5.8 mm) were reconstructed after a high-frequency cutoff with a Butterworth filter.

The easy Z-Score Imaging System (eZIS; Fuji Film RI Pharma), used for the statistical analysis of SPECT images, standardizes brain images using Statistical Parametric Mapping (SPM99) [24]. Each SPECT image of the subjects after anatomical standardization followed by isotropic 12-mm smoothing was compared with the mean and SD of SPECT images of the age-matched healthy controls already incorporated in the eZIS program as a normal database using voxel-by-voxel Z-score analysis after voxel normalization to global mean values: Z score = (control mean − individual value)/control SD. These Z-score maps were overlain on tomographic sections and projection with an averaged Z-score of 14-mm thickness to surface rendering of the anatomically standardized MRI template.

Positron emission tomography (PET) was performed in Patients 2 and 3, 1 h after administering [^{18}F]-fluorodeoxyglucose (^{18}FDG) (approximately 3 MBq/kg of body weight) using a Biograph Duo, ECAT EXACT HR$^+$ (Siemens, Hoffman Estates, IL) or SET-2400 W (Shimadzu) after fasting for at least 4 h. Emission scans were performed for 10 min for the entire brain. Attenuation was corrected. Fourteen 6-mm-thick slices parallel to the orbitomeatal line, encompassing virtually the entire brain, were analyzed visually by two investigators independently. When the interpretation was inconsistent, a third investigator was called to make a decision.

2.3. Gene analysis

Gene analyses were performed with the informed consent of the patients' parents. Genomic DNA was extracted from peripheral blood lymphocytes using a Sepa Gene kit (Sanko Junyaku, Tokyo, Japan). All coding exons and flanking introns in *NKX2-1* were amplified by PCR. All primers were based on the NCBI reference sequence (accession number NG_013365; the primer sequences are available upon request). The PCR products were separated on 3% agarose gels and purified with a QIAquick Gel Extraction kit (QIAGEN, Chatsworth, CA, USA). The PCR products were sequenced directly using a Big Dye Primer Cycle Sequencing kit and ABI 310 Genetic Analyzer (PE Applied Biosystems, Foster City, CA, USA).

Subsequent array-based comparative genomic hybridization (CGH) analysis was performed using an Agilent 244 K oligonucleotide array (Agilent, Santa Clara, CA; www.agilent.com) with a resolution of approximately 15 kb following the protocols provided by Agilent. The array was analyzed with the Agilent scanner and the Feature Extraction software (v. 9.1.3).

3. Results

From the raw nuclear image ECD-SPECT findings in all three patients (Fig. 2, lower figures) and FDG-PET in Patients 2 and 3

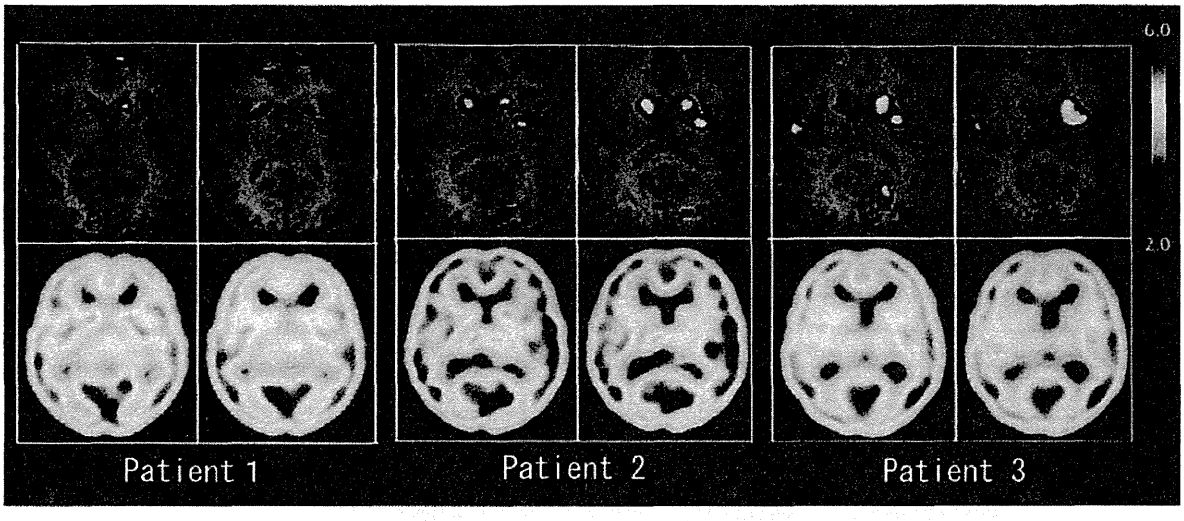

Fig. 2. ECD-SPECT and eZIS results.Usual color images of ECD-SPECT in three patients were shown on the lower figures in each patient. Analyzed images using eZIS were shown on the upper figures. The converted images indicate regions of decreased cerebral blood flow by colors from blue (2.0 standard deviation) to red (6.0 standard deviation). Reduction in cerebral blood flow was shown most common and prominent in the bilateral caudate nuclei in all three patients.

(data not shown), we could not discriminate visible areas of abnormal cerebral perfusion or glucose metabolism. However, the statistical analysis of the ECD-SPECT data using eZIS demonstrated significant declines in cerebral blood flow in the basal ganglia, especially in the caudate nuclei (Fig. 2, upper figure). Although several other brain regions were shown to have decreased blood flow, these were not shared in the three patients.

Array CGH analysis revealed that Patient 1 had an approximately 2.6-Mb hemizygous deletion including *NKX2-1* in 14q12–13 (Fig. 3, top). Direct sequencing analysis revealed a novel hemizygous mutation in the coding exons in Patients 2 and 3 (Fig. 3, bottom), but no mutation in Patient 1. A hemizygous G-to-T substitution at nucleotide position 613 (c.613G > T) in Patients 2 and 3 created an amino acid substitution at amino acid position 205 (p.Val205Phe) within exon 3, which is localized within the *NKX2-1* homeodomain. The mothers and grandmother of Patients 2 and 3 had the same missense mutation.

4. Discussion

In this study, we diagnosed three children with brain–lung–thyroid syndrome based on clinical findings of delayed walking, unsteady gait, choreoathetosis, and hypothyroidism. The diagnosis was confirmed by genetic analysis detecting a novel hemizygous deletion and missense mutations in *NKX2-1*. In addition, we performed nuclear image examinations and analyzed the results using statistical image analysis with eZIS. We found a significant reduction in the blood flow in the caudate nuclei in all three patients.

Recurrent respiratory infection was observed only in the patient with the deletion in *NKX2-1*, but not in the two patients with missense mutations. These phenotype-genotype correlations support previous reports [8,10–13] that large deletions and truncation mutations are related to the severe phenotype with the symptom triad, while missense mutations have a milder phenotype [13]. The existence of respiratory symptoms is very important for management because no deaths have been reported in patients without lung disease [12]. In one case with a missense mutation, hypothyroidism was not detected until the age of 5 years, while it was detected in his cousin with the same mutation at neonatal screening. This interfamilial heterogeneity, as described previously [25], indicates that simple haploinsufficiency cannot fully explain the spectrum of clinical presentations. Other modifying genes might contribute to the phenotype heterogeneity [9,12].

Central nervous impairment is the most common and essential symptom in brain–lung–thyroid syndrome [12,13]. Typically, mental retardation and brain MRI abnormalities are not associated with this disease. The characteristic presentation involves delayed walking, a staggering gait, and choreoathetosis. Since no obvious nervous system abnormalities were detected on neurological examinations, we speculate that the choreoathetosis in the lower limbs caused the delay in walking and unsteady gait.

To identify the brain region responsible for the neurological impairment, we examined brain ECD-SPECT and FDG-PET, but no obvious pathological abnormalities were detected on visual inspection of the raw images. Further statistical analysis of the ECD-SPECT data was performed using eZIS, while the FDG-PET was not analyzed because we did not have an appropriate analysis method. The eZIS method can detect a significant difference of regional cerebral blood flow by comparison with age-matched normal controls, and shows the result as color images. Previous reports described significant superiority of this program over visual inspection of raw SPECT images in several diseases [26–28]. We analyzed our patients and found a common, significant reduction in cerebral blood flow in the caudate nuclei. Although most reports describe expression of the *NKX2-1* gene in the pallidum [8,21,22], a recent study showed *NKX2-1* expression in the postnatal mouse striatum, including the caudate nuclei, in addition to the pallidum [29]. In humans, nuclear image studies indicated a reduction in blood flow [23] and glucose metabolism [15] in the basal ganglia. Hypoperfusion in the caudate nuclei was described in a patient with Huntington's disease [30,31], which usually involves chorea. From these reports and our ECD-SPECT findings using eZIS, we believe that the region responsible for the neurological symptoms in brain–lung–thyroid syndrome, pathologically, is the caudate nuclei. We speculate the possible mechanism that the mutation may impair developmental differentiation and organization of the striatum. Huntington's disease, which also involves the caudate nuclei, partially mimics brain–lung–thyroid syndrome clinically, although the latter is easily differentiated by the history of delayed walking.

In our cases, oral L-dopa [32], a dopamine agonist, and clonazepam failed to improve their neurological impairment. Only a few effective treatment for involuntary movement has been reported [13]. Although some reports described the choreatic movements tend to decrease over time [7,23], the movement disability causes severe trouble with daily life, especially writing difficulty resulting in a leaning impairment in

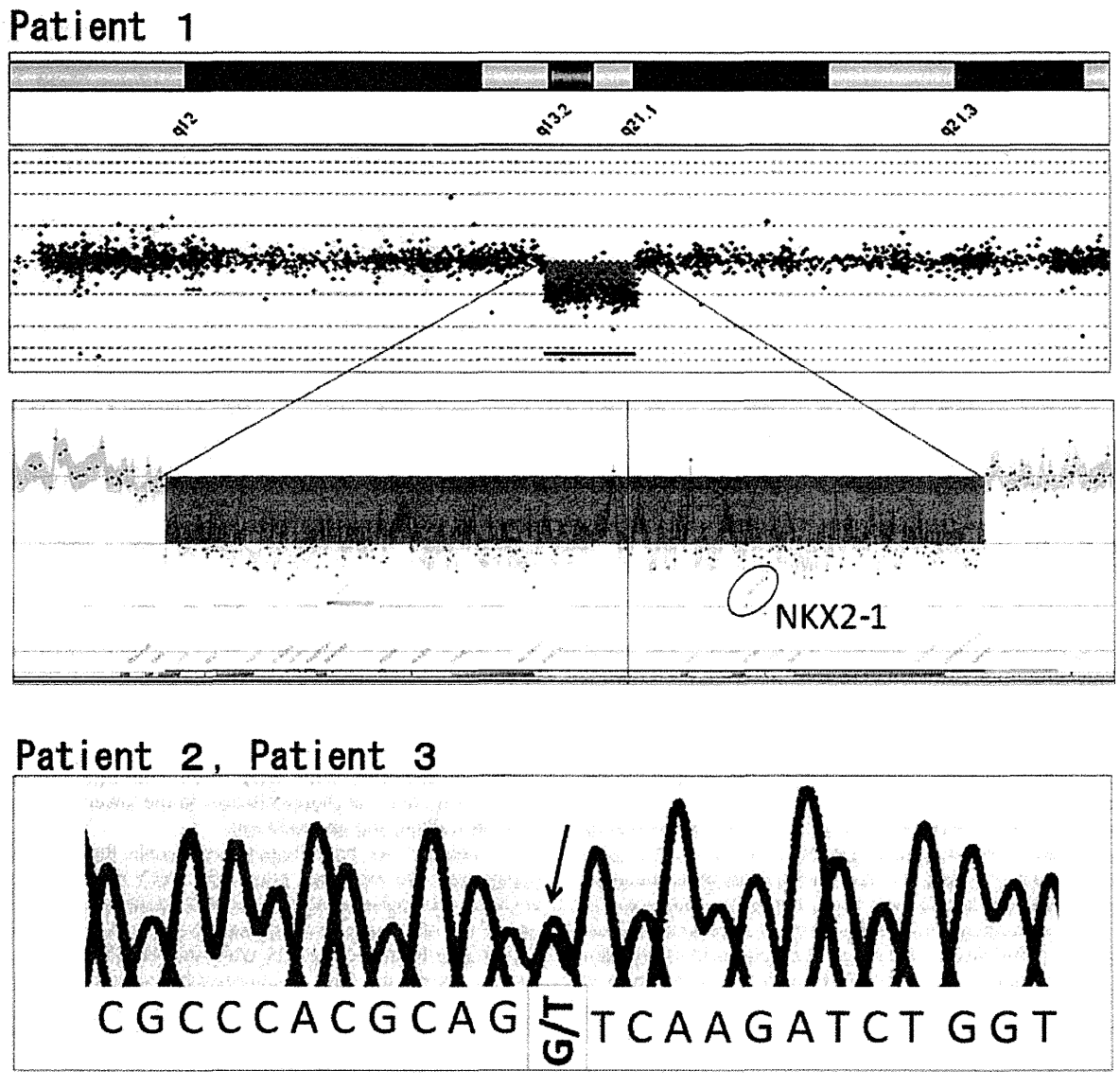

Fig. 3. Deletion and missense mutation in *NKX2-1*. Chromosome 14 profile and detail of 14q12–13 region generated by Cytogenomics (version 1.5, Agilent Technologies) showed a hemizygous 2.6-Mb deletion including *NKX2-1* in Patient 1. Sequencing analysis showed hemizygous missense mutations (c.613G>T) in *NKX2-1* in Patients 2 and 3.

childhood. We postulate that deep brain stimulation might treat involuntary movement, such as in Huntington's disease [33]. The pathophysiology of this disease should be clarified to develop an effective treatment.

Acknowledgments

We are grateful to Ms. Yoko Chiba and Ms. Kumi Itou for their technical assistance.

References

[1] Hamdan H, Liu H, Li C, Jones C, Lee M, deLemos R, et al. Structure of the human Nkx2.1 gene. Biochim Biophys Acta 1998;1396:336–48.
[2] Ikeda K, Clark JC, Shaw-White JR, Stahlman MT, Boutell CJ, Whitsett JA. Gene structure and expression of human thyroid transcription factor-1 in respiratory epithelial cells. J Biol Chem 1995;270:8108–14.
[3] Lazzaro D, Price M, de Felice M, Di Lauro R. The transcription factor TTF-1 is expressed at the onset of thyroid and lung morphogenesis and in restricted regions of the foetal brain. Development 1991;113:1093–104.
[4] Kimura S, Hara Y, Pineau T, Fernandez-Salguero P, Fox CH, Ward JM, et al. The T/ebp null mouse: thyroid-specific enhancer-binding protein is essential for the organogenesis of the thyroid, lung, ventral forebrain, and pituitary. Genes Dev 1996;10:60–9.
[5] Puelles L, Kuwana E, Puelles E, Bulfone A, Shimamura K, Keleher J, et al. Pallial and subpallial derivatives in the embryonic chick and mouse telencephalon, traced by the expression of the genes Dlx-2, Emx-1, Nkx-2.1, Pax-6, and Tbr-1. J Comp Neurol 2000;424:409–38.
[6] Acebron A, Aza-Blanc P, Rossi DL, Lamas L, Santisteban P. Congenital human thyroglobulin defect due to low expression of the thyroid-specific transcription factor TTF-1. J Clin Invest 1995;96:781–5.
[7] Breedveld GJ, van Dongen JW, Danesino C, Guala A, Percy AK, Dure LS, et al. Mutations in TITF-1 are associated with benign hereditary chorea. Hum Mol Genet 2002;11:971–9.
[8] Krude H, Schutz B, Biebermann H, von Moers A, Schnabel D, Neitzel H, et al. Choreoathetosis, hypothyroidism, and pulmonary alterations due to human NKX2-1 haploinsufficiency. J Clin Invest 2002;109:475–80.
[9] Breedveld GJ, Percy AK, MacDonald ME, de Vries BB, Yapijakis C, Dure LS, et al. Clinical and genetic heterogeneity in benign hereditary chorea. Neurology 2002;59:579–84.
[10] Willemsen MA, Breedveld GJ, Wouda S, Otten BJ, Yntema JL, Lammens M, et al. Brain-thyroid-lung syndrome: a patient with a severe multi-system disorder due to a de novo mutation in the thyroid transcription factor 1 gene. Eur J Pediatr 2005;164:28–30.
[11] Kleiner-Fisman G, Lang AE. Benign hereditary chorea revisited: a journey to understanding. Mov Disord 2007;22:2297–305 [quiz 452].
[12] Carre A, Szinnai G, Castanet M, Sura-Trueba S, Tron E, Broutin-L'Hermite I, et al. Five new TTF1/NKX2.1 mutations in brain–lung–thyroid syndrome: rescue by PAX8 synergism in one case. Hum Mol Genet 2009;18:2266–76.

[13] Inzelberg R, Weinberger M, Gak E. Benign hereditary chorea: an update. Parkinsonism Relat Disord 2011;17:301–7.
[14] Carmo Costa M, Costa C, Silva AP, Evangelista P, Santos L, Ferro A, et al. Nonsense mutation in TITF1 in a Portuguese family with benign hereditary chorea. Neurogenetics 2005;6:209–15.
[15] Salvatore E, Di Maio L, Filla A, Ferrara AM, Rinaldi C, Sacca F, et al. Benign hereditary chorea: clinical and neuroimaging features in an Italian family. Mov Disord 2010;25:1491–6.
[16] Butt SJB, Sousa VH, Fuccillo MV, Hjerling-Leffler J, Miyoshi G, Kimura S, et al. The requirement of Nkx2-1 in the temporal specification of cortical interneuron subtypes. Neuron 2008;59:722–32.
[17] Trueba SS, PAX8, TITF1, and FOXE1 gene expression patterns during human development: new insights into human thyroid development and thyroid dysgenesis-associated malformations. J Clin Endocrinol Metabol 2004;90:455–62.
[18] Maeda Y, Davé V, Whitsett J. Transcriptional control of lung morphogenesis. Physiol Rev 2007;87:219–44.
[19] Guillot L, Carré A, Szinnai G, Castanet M, Tron E, Jaubert F, et al. NKX2-1mutations leading to surfactant protein promoter dysregulation cause interstitial lung disease in "Brain–Lung–Thyroid Syndrome". Hum Mutat 2010;31:E1146–62.
[20] Glik A, Vuillaume I, Devos D, Inzelberg R. Psychosis, short stature in benign hereditary chorea: a novel thyroid transcription factor-1 mutation. Mov Disord 2008;23:1744–7.
[21] Sussel L, Marin O, Kimura S, Rubenstein JL. Loss of Nkx2.1 homeobox gene function results in a ventral to dorsal molecular respecification within the basal telencephalon: evidence for a transformation of the pallidum into the striatum. Development 1999;126:3359–70.
[22] Flandin P, Kimura S, Rubenstein JLR. The progenitor zone of the ventral medial ganglionic eminence requires Nkx2-1 to generate most of the globus pallidus but few neocortical interneurons. J Neurosci 2010;30:2812–23.
[23] Mahajnah M, Inbar D, Steinmetz A, Heutink P, Breedveld GJ, Straussberg R. Benign hereditary chorea: clinical, neuroimaging, and genetic findings. J Child Neurol 2007;22:1231–4.
[24] Kanetaka H, Matsuda H, Asada T, Ohnishi T, Yamashita F, Imabayashi E, et al. Effects of partial volume correction on discrimination between very early Alzheimer's dementia and controls using brain perfusion SPECT. Eur J Nucl Med Mol Imaging 2004;31:975–80.
[25] Montanelli L, Tonacchera M. Genetics and phenomics of hypothyroidism and thyroid dys- and agenesis due to PAX8 and TTF1 mutations. Mol Cell Endocrinol 2010;322:64–71.
[26] Matsuda H, Mizumura S, Nagao T, Ota T, Iizuka T, Nemoto K, et al. Automated discrimination between very early Alzheimer disease and controls using an easy Z-score imaging system for multicenter brain perfusion single-photon emission tomography. AJNR Am J Neuroradiol 2007;28:731–6.
[27] Imamura K, Wada-Isoe K, Kowa H, Tanabe Y, Nakashima K. The effect of donepezil on increased regional cerebral blood flow in the posterior cingulate cortex of a patient with Parkinson's disease dementia. Neurocase 2008;14:271–5.
[28] Sasaki M, Nakagawa E, Sugai K, Shimizu Y, Hattori A, Nonoda Y, et al. Brain perfusion SPECT and EEG findings in children with autism spectrum disorders and medically intractable epilepsy. Brain Dev 2010;32:776–82.
[29] Magno L, Catanzariti V, Nitsch R, Krude H, Naumann T. Ongoing expression of Nkx2.1 in the postnatal mouse forebrain: potential for understanding NKX2.1 haploinsufficiency in humans? Brain Res 2009;1304:164–86.
[30] Hasselbalch SG, Oberg G, Sorensen SA, Andersen AR, Waldemar G, Schmidt JF, et al. Reduced regional cerebral blood flow in Huntington's disease studied by SPECT. J Neurol Neurosurg Psychiatry 1992;55:1018–23.
[31] Reynolds Jr NC, Hellman RS, Tikofsky RS, Prost RW, Mark LP, Elejalde BR, et al. Single photon emission computerized tomography (SPECT) in detecting neurodegeneration in Huntington's disease. Nucl Med Commun 2002;23:13–8.
[32] Asmus F, Horber V, Pohlenz J, Schwabe D, Zimprich A, Munz M, et al. A novel TITF-1 mutation causes benign hereditary chorea with response to levodopa. Neurology 2005;64:1952–4.
[33] Kang GA, Heath S, Rothlind J, Starr PA. Long-term follow-up of pallidal deep brain stimulation in two cases of Huntington's disease. J Neurol Neurosurg Psychiatry 2010;82:272–7.

Molecular Genetics and Metabolism 105 (2012) 553–558

Contents lists available at SciVerse ScienceDirect

Molecular Genetics and Metabolism

journal homepage: www.elsevier.com/locate/ymgme

Simple and rapid genetic testing for citrin deficiency by screening 11 prevalent mutations in *SLC25A13*

Atsuo Kikuchi [a,*], Natsuko Arai-Ichinoi [a], Osamu Sakamoto [a], Yoichi Matsubara [b], Takeyori Saheki [c,1], Keiko Kobayashi [d], Toshihro Ohura [e], Shigeo Kure [a]

[a] Department of Pediatrics, Tohoku University Graduate School of Medicine, 1-1 Seiryo-machi, Aoba-ku, Sendai, Miyagi 980-8574, Japan
[b] Department of Medical Genetics, Tohoku University School of Medicine, 1-1 Seiryo-machi, Aoba-ku, Sendai, Miyagi 980-8574, Japan
[c] Institute for Health Sciences, Tokushima Bunri University, 180 Yamashiro-cho, Tokushima 770-8514, Japan
[d] Department of Molecular Metabolism and Biochemical Genetics, Kagoshima University, Kagoshima 890-8544, Japan
[e] Division of Pediatrics, Sendai City Hospital, 3-1 Shimizukoji, Wakabayashi-ku, Sendai, Miyagi 984-8501, Japan

ARTICLE INFO

Article history:
Received 13 November 2011
Received in revised form 29 December 2011
Accepted 30 December 2011
Available online 8 January 2012

Keywords:
Citrin deficiency
Genetic diagnosis
Rapid diagnosis
Expanded newborn screening
SLC25A13

ABSTRACT

Citrin deficiency is an autosomal recessive disorder caused by mutations in the *SLC25A13* gene and has two disease outcomes: adult-onset type II citrullinemia and neonatal intrahepatic cholestasis caused by citrin deficiency. The clinical appearance of these diseases is variable, ranging from almost no symptoms to coma, brain edema, and severe liver failure. Genetic testing for *SLC25A13* mutations is essential for the diagnosis of citrin deficiency because chemical diagnoses are prohibitively difficult. Eleven *SLC25A13* mutations account for 95% of the mutant alleles in Japanese patients with citrin deficiency. Therefore, a simple test for these mutations is desirable. We established a 1-hour, closed-tube assay for the 11 *SLC25A13* mutations using real-time PCR. Each mutation site was amplified by PCR followed by a melting-curve analysis with adjacent hybridization probes (HybProbe, Roche). The 11 prevalent mutations were detected in seven PCR reactions. Six reactions were used to detect a single mutation each, and one reaction was used to detect five mutations that are clustered in a 21-bp region in exon 17. To test the reliability, we used this method to genotype blind DNA samples from 50 patients with citrin deficiency. Our results were in complete agreement those obtained using previously established methods. Furthermore, the mutations could be detected without difficulty using dried blood samples collected on filter paper. Therefore, this assay could be used for newborn screening and for facilitating the genetic diagnosis of citrin deficiency, especially in East Asian populations.

1. Introduction

Citrin deficiency is an autosomal recessive disorder that results from mutations in the *SLC25A13* gene [1] and causes two diseases: adult-onset type II citrullinemia (CTLN2; OMIM #603471) and neonatal intrahepatic cholestasis caused by citrin deficiency (NICCD; OMIM#605814) [1–4]. The clinical appearance of these diseases is variable and ranges from almost no symptoms to coma, brain edema, and severe liver failure requiring transplantation [5–8]. In a study of patients with NICCD, only 40% of individuals were identified by newborn screenings to have abnormalities, such as hypergalactosemia, hypermethioninemia, and hyperphenylalaninemia [9]. Other patients were referred to hospitals with suspected neonatal hepatitis or biliary atresia, due to jaundice or discolored stool [9]. Hypercitrullinemia was not observed in all patients [9]. Mutation analysis of *SLC25A13* is indispensable because of the difficulties associated with the chemical diagnosis of citrin deficiency. The *SLC25A13* mutation spectrum in citrin deficiency is heterogeneous, and more than 31 mutations of *SLC25A13* have been identified to date [1,10–18]. However, there are several predominant mutations in patients from East Asia. As shown in Table 1, 6 prevalent mutations account for 91% of the mutant alleles in the Japanese population [12,19]. Five additional mutations also occur within a 21-bp cluster in exon 17 (Table 1 and Fig. 1D). The six prevalent mutations, together with the five mutations in exon 17, account for 95% of the mutant alleles in Japan [12,19].

Several different methods, such as direct sequencing, PCR restriction fragment length polymorphism (PCR-RFLP), and denaturing high performance liquid chromatography (DHPLC), are currently used for the detection of mutations in *SLC25A13* [1,10–14,19]. However, these methods are too complex for clinical use. Direct sequencing is a standard but cumbersome method. The PCR-RFLP method is

Abbreviations: CTLN2, adult-onset type II citrullinemia; FRET, fluorescence resonance energy transfer; HRM, high resolution melting; NICCD, neonatal intrahepatic cholestasis caused by citrin deficiency; Tm, melting temperature.

* Corresponding author. Fax: +81 22 717 7290.
E-mail address: akikuchi-thk@umin.ac.jp (A. Kikuchi).
[1] Present address: Institute of Resource Development and Analysis, Kumamoto University, Kumamoto 860-0811, Japan.

1096-7192/$ – see front matter © 2012 Elsevier Inc. All rights reserved.
doi:10.1016/j.ymgme.2011.12.024

Table 1
Seven primer/probe sets and 11 targeted mutations of *SLC25A13*.

Primer/probe set	Mutation		Location	Nucleotide change	Effects of mutations	Allele frequency*[19]	References
A	Mutation [I]	:851del4	exon 9	c.851_854delGTAT	p.R284fs(286X)	33.2%	[1]
B	Mutation [II]	:g.IVS11+1G>A	intron 11	c.1019_1177del	p.340_392del	37.6%	[1]
C	Mutation [III]	:1638ins23	exon 16	c.1638_1660dup	p.A554fs(570X)	3.4%	[1]
D	Mutation [IV]	:S225X	exon 7	c.675C>A	p.S225X	5.3%	[1]
E	Mutation [V]	:g.IVS13+1G>A	intron 13	c.1231_1311del	p.411_437del	8.2%	[1]
F	Mutation [XIX]	:IVS16ins3kb	intron 16	c. aberrant RNA	p.A584fs(585X)	4.6%	[19]
G	Mutation [VI]	:1800ins1	exon 17	c.1799_1800insA	p.Y600X	1.3%	[10]
	Mutation [VII]	:R605X	exon 17	c.1813C>T	p.R605X	0.90%	[10]
	Mutation [VIII]	:E601X	exon 17	c.1801G>T	p.E601X	1.2%	[11]
	Mutation [IX]	:E601K	exon 17	c.1801G>A	p.E601K	0.30%	[11]
	Mutation [XXI]	:L598R	exon 17	c.1793T>G	p.L598R	0%	[15]
						Total 95.1%	

* The frequency of each mutant allele among Japanese patients with citrin deficiency.

complicated and can lead to genotyping errors, due to incomplete digestion by the restriction enzymes. DHPLC is time-consuming and requires expensive equipment. Thus, there is a strong need for the development of a simple test for these mutations.

The goal of this study was to establish a rapid and simple test for the detection of the 11 most common *SLC25A13* mutations. We adopted the HybProbe format (Roche) for the detection of the mutations using real-time PCR followed by a melting-curve analysis with adjacent hybridization probes [20,21]. This assay can be completed in less than 1 h and has the advantage of being a closed-tube assay. The fundamental process for detecting point mutations using the HybProbe assay is presented in Fig. 1A. The 11 prevalent mutations contain not only point mutations but also include a 4-bp deletion and insertions of 1-bp, 23-bp and 3-kb genomic fragments (Table 1 and Fig. 1). Careful design of the PCR primers and HybProbes enabled us to test for these various *SLC25A13* mutations.

2. Methods

2.1. Subjects

CTLN2 and NICCD were diagnosed, as previously described [9,10,19,22–24]. Genomic DNA of the patients was obtained from peripheral blood leukocytes using the DNeasy blood kit (Qiagen Inc., Valencia, CA, USA). Genomic DNA was purified from filter paper blood samples using the ReadyAmp Genomic DNA Purification System (Promega, Madison, WI, USA). Mutations in these DNA samples were analyzed at Kagoshima University using a combination of PCR with or without restriction enzyme digestion or by direct sequencing, as previously described [1,10–14,19]. Another set of samples was obtained from 420 healthy volunteers (mainly from Miyagi prefecture in the northeastern region of Japan) at Tohoku University. Genomic DNA from leukocytes was extracted, as described above.

2.2. Detection of seven prevalent mutations in *SLC25A13* using the HybProbe assay

HybProbe probes comprise a pair of donor and acceptor oligonucleotide probes designed to hybridize adjacent to their target sites in an amplified DNA fragment [20,21]. The donor probes are labeled at their 3′ end with fluorescein isothiocyanate (FITC), whereas the acceptor probes are labeled at their 5′ end with LC Red640; these acceptor probes are phosphorylated at their 3′ end to prevent extension by the DNA polymerase. When two probes hybridize to the amplicon, the fluorescent dyes are located within 5 bases of each other, which allows fluorescence resonance energy transfer (FRET) between the excited FITC and the LC Red640; this process emits light that can be quantified by real-time PCR. Following PCR amplification, a melting-peak analysis is performed. The melting peak is produced by the reporter probe, which has a lower melting temperature (Tm) than the other probe, called the anchor probe. As the reporter melts from the target, the fluorophores are separated, and the FRET ceases. The Tm of the reporter probe determines the reaction

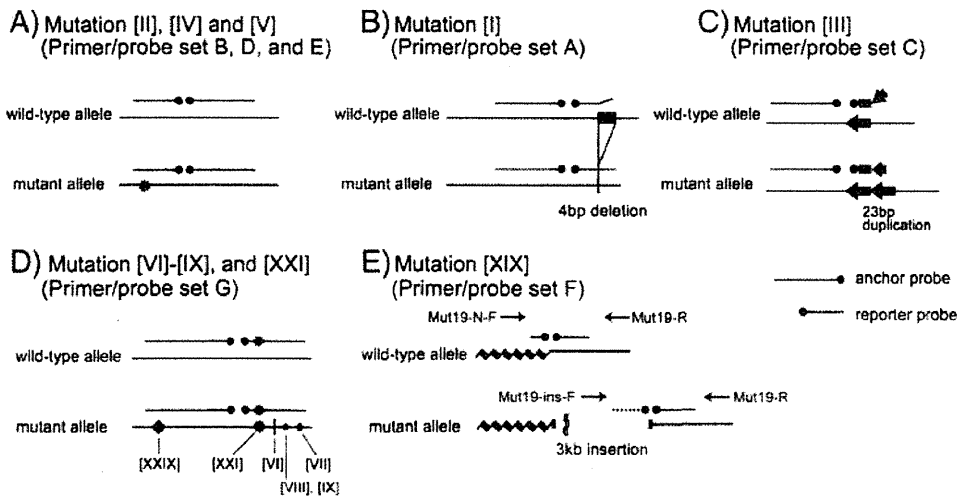

Fig. 1. Principle of *SLC25A13* mutation detection by melting-curve analysis with the HybProbe assay. In primer/probe sets A–E, and G, PCR was performed with a pair of primers, whereas in primer/probe set F, two forward primers and one common reverse primer were used for the amplification of both wild-type and mutant alleles. Note that mutation [XXIX], located on the anchor probe of primer/probe set G, is a non-target mutation.

specificity (i.e., binding of the probe to a perfectly matched sequence rather than to regions with sequence mismatches).

Seven primer/probe sets were designed for this study. Fig. 1 shows a schematic diagram of the strategy for mutation detection using these primer/probe sets. Tables 1 and 2 list the primer/probe sets and corresponding sequences and primer concentrations that were used to target the 11 mutations. Primer/probe sets A, B, C, D, E, and F were designed to detect mutations [I], [II], [III], [IV], [V], and [XIX], respectively. Primer/probe set G was designed to detect the five mutations clustered on exon 17: mutations [VI], [VII], [VIII], [IX], and [XXI] (Fig. 1D). All primers and probes were synthesized based on the NCBI reference SLC25A13 gene sequence (GenBank accession no. **NM_014251**) with the exception of mutation [XIX]:IVS16ins3kb, which was designed according to [19].

Real-time PCR and subsequent melting curve analyses were performed in a closed tube using a 20-μL mixture on a LightCycler 1.5 (Roche Diagnostics, Tokyo, Japan). The PCR mixture contained 2.0 μL of genomic DNA (10–50 ng), 0.5 μM of forward primer, 0.5 or 0.1 μM of reverse primer, 0.2 μM of each sensor and anchor probe, and 10 μL of Premix ExTaq™ (Perfect Real Time) reagent (TaKaRa Bio Inc., Otsu, Japan).

The thermal profile conditions were identical for all seven assays and consisted of an initial denaturation step (30 s at 95 °C), followed by 45 amplification cycles with the following conditions: denaturation for 5 s at 95 °C and annealing and extension for 20 s at 60 °C. The transition rate between all steps was 20 °C/s. After amplification, the samples were held at 37 °C for 1 min, followed by the melting curve acquisition at a ramp rate of 0.15 °C/s extending to 80 °C with continuous fluorescence acquisition.

Table 2
Primers, probes and target amplicon sequences, target mutation sites, and primer concentrations.

Primer/probe set	Name	Sequences of PCR products, primer locations, probe sequences, and mutation sites (5′ to 3′)	Concentration (μmol/L)
A		GGCTATACTGAAATATGAGAAatgaaaaaagggatgtttttaaattttataatgtaaattgtaataaattggtatatttgttgcttgtgtttgtttttcccctacagac	
		gtatgaccttagcagacattgaacggattgctcctctggaagagggaactctgccCTTTAACTTGGCTGAGG (181 bp)	
	Mut1-F	GGCTATACTGAAATATGAGAA	0.5
	Mut1-R	CCTCAGCCAAGTTAAAG	0.5
	Mut1-UP	ATGTAAATTGTAATAAATTGGTATATTTGTTGCTTGTGTT-FITC	
	Mut1-DW	LC Red640-GTTTTTCCCCTACAGAC**GACC**-P	
B		GAATGCAGAACCAACGAtcaactggctcttttgtgggagaactcatgtataaaaacagctttgactgttttaagaaagtgctacgctatgaaggcttctt	
		tggactgtatagaggttagtgccacatgctcaatacctgttaggtgaaataacactcaaaggtttggtttctcatcttagtgcctGACATGAATTAGCAAGACTG (205 bp)	
	Mut2-F	GAATGCAGAACCAACGA	0.5
	Mut2-R	CAGTCTTGCTAATTCATGTC	0.1
	Mut2-UP	ACCTAACAGGTATTGAGCATGTG-FITC	
	MUt2-DW	LC Red640-CACTAA**CCT**CTATACAGTCCA-P	
C		GCAGTTCAAAGCACAGTTATTttatatagtgagaatgtgaccagactgagatggtgttgtgtctctcctgcaggtatgcctgcagcatctttagtg	
		acccctgctgatgttatcaagacgagattacaggtg	
		gctgcccggg(**gagatta**caggtggctgcccggg)ctggccaaaccaCTTACAGCGGAGTGATAGAC (175 bp)	
	Mut3-F	GCAGTTCAAAGCACAGTTATT	0.5
	Mut3-R	GTCTATCACTCCGCTGTAAG	0.5
	Mut3-UP	ACCCCTGCTGATGTTATCAAGACGAGATTACAGGT-FITC	
	Mut3-DW	LC Red640-GCTGCCCGGG**GAGATTA**-P	
D		TCAATTTATTTGAGGCTGCtggaggtaccacatcccatcaagttagtttctcctattttaatggatttaattcgctccttaacaac	
		atggaactcattagaaagatctatagcactc	
		tggctggcaccaggaaagatgttgaagtGACTAAGGGTGAGTGAGAA (164 bp)	
	Mut4-F	TCAATTTATTTGAGGCTGC	0.5
	Mut4-R	TTCTCACTCACCCTTAGTC	0.5
	Mut4-UP	AATGGATTTAATT**C**GCTCCTTAACA-FITC	
	Mut4-DW	LC Red640-ATGGAACTCATTAGAAAGATCTATAGCACTC-P	
E		TGCACAAAGATGGTTCGgtcccacttgcagcagaaattcttgctggaggctgc**g**taagtacctttgaagctctcttcattgaaaagacttgtttcac	
		atatatatcactaccatggtcaacaggtgtggactaaggcttctgttTAACCACAGATCCTGCA (162 bp)	
	Mut5-F	TGCACAAAGATGGTTCG	0.5
	Mut5-R	TGCAGGATCTGTGGTTA	0.5
	Mut5-UP	GTGAAACAAGTCTTTTCAATGAAGAGAGCTTC-FITC	
	Mut5-DW	LC Red640-AAGGTACTTA**C**GCAGCCTC-P	
F	normal allele	GGAGCTGGTGGTATGGAAataatgtgttcttaactaactctttggtatcaggtaaatttttaaaatatctaattatatctgtgatttctc	
		catttttttaaagctcgtgtatttcgatcctcaccccagtttggt	
		gtaactttgctgacttacgaattgctacagcgatggttctacattgattttggaggagtgtaagtatcatgctaaatctgctgctaaatttt	
		GGCTGCTGCTAATGCTC (244 bp)	
	insertion allele	CCATCTTCCTCCTCCCTTggcagccccgccccccgatttctccatttttttaaagctcgtgtatttcgatcctcaccccagtttggt	
		gtaactttgctgacttacgaattgctacagcgatggttctacattgatttt	
		ggaggagtgtaagtatcatgctaaatctgctgctaaattttGGCTGCTGCTAATGCTC (196 bp)	
	Mut19-N-F	GGAGCTGGTGGTATGGAA	0.5
	Mut19-ins-F	CCATCTTCCTCCTCCCTT	0.5
	Mut19-R	GAGCATTAGCAGCAGCC	0.5
	Mut19-UP	ACCAAACTGGGGTGAGGATCGAAATACACGAGCTTTAAAAAAATG-FITC	
	Mut19-N-DW	LC Red640-AGAAATCACAGATATAATTAGATATTT-P	
	Mut19-ins-DW	LC Red640-AGAAATCGGGGGGCGGGG-P	
G		TCTTAACTAACTCTTTGGTATCAGGTaaatttttaaaatatctaattatatctgtgatttctccatttttttaaagctcg	
		tgtatttcgatcctcaccccagtttggtgtaacttt**g**ct**g**actt**a(a)cg**aattgctacag**c**ga	
		tggttctacattgatttt**g**gaggagtgtaagtatcatgctaaatctgctgctaaattttGGCTGCTGCTAATGCTC (217 bp)	
	Mut6-9, 21-F	TCTTAACTAACTCTTTGGTATCAGGT	0.5
	Mut6-9, 21-R	GAGCATTAGCAGCAGCC	0.5
	Mut6-9, 21-UP	TGTATTTCGATCCTCACCCCAGTTTGGTGTAACTT-FITC	
	Mut6-9, 21-DW	LC Red640-GC**G**GACTT**ACG**AATTGCTACAG**C**GA-P	

Upper case and underlined letters indicate the locations of primers and probes, respectively. Inserted DNA is shown in parenthesis. Nucleotides in boldface were used for mutation detection.
F: forward, R: reverse, UP: upstream, DW: downstream, N: normal allele, ins: insertion allele, FITC: fluorescein isothiocyanate, P: phosphate.

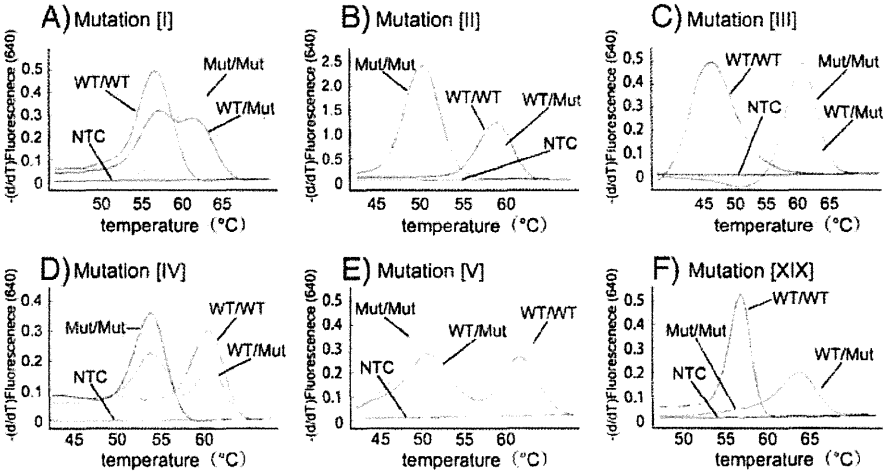

Fig. 2. Typical melting curves used in the detection of mutations [I–V] and [XIX]. Each assay using primer/probe sets A–F is displayed in a separate graph (A–F). WT: wild-type allele, Mut: mutant allele, NTC: no DNA template control.

2.3. Validation of the mutation detection system

After establishing the protocol for detecting the 11 prevalent mutations, 50 DNA samples from patients' blood were sent from Kagoshima University to Tohoku University for the validation of this system in a single-blind manner. Similarly, 26 DNA samples purified from paper-filter blood samples were analyzed in the same manner as the blood DNA samples.

2.4. Estimation of the carrier frequency

For the estimation of the heterozygous carrier frequency, 420 genomic DNA samples from healthy volunteers were screened using the HybProbe analysis for the 11 prevalent mutations. All detected mutations were confirmed by direct sequencing.

2.5. Ethics

This study was approved by the Ethical Committees of Tohoku University School of Medicine and Kagoshima University. Written informed consent was obtained from all participants or their guardians.

3. Results

3.1. Development of the mutation detection system

In primer/probe sets B, D, and E, the reporter probes were designed to be complimentary to the wild-type allele (Fig. 1A). To allow for an improved detection of the mutations, primer/probe sets A and C were designed to be complementary to the mutant allele (Figs. 1B, C). In the primer/probe set F, two forward PCR primers, which were specific to the wild-type and the mutant alleles, were used with a common reverse primer for the co-amplification of the wild-type and 3-kb insertion alleles (Fig. 1E). Two reporter probes, which had a common anchor probe, were used for the detection of the wild-type and mutant alleles. Because the two reporter probes had different melting temperatures, we were able to identify the allele that was amplified. Fig. 2 shows representative results of the melting curve analyses using the primer/probe sets A–F, in which all of the mutant alleles generated distinct peaks corresponding to the wild-type alleles.

In the primer/probe set G, we used a reporter probe that was complementary to the mutant [XXI] allele (Fig. 1D). All five mutations in exon 17 were successfully differentiated from the wild-type allele (Figs. 3A–E). The [XXIX] mutation is an additional mutation in exon

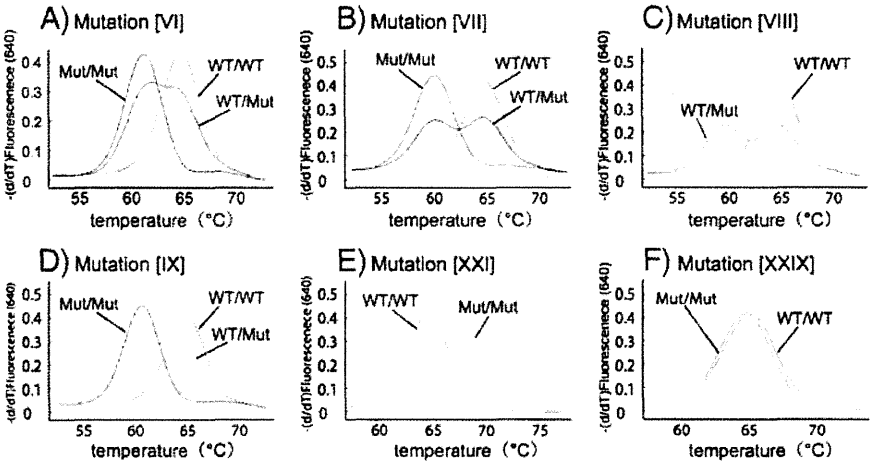

Fig. 3. Typical melting curves used in the detection of mutations [VI–XI], [XXI], and [XXIX] on exon 17. Genotyping was performed using primer/probe set G. Each melting curve for a target mutation is displayed in a separate graph (A–F). Note that mutation [XXIX] (F) is a non-target mutation on the anchor probe. WT: wild-type allele, Mut: mutant allele.

17 that is not listed in Table 1. The [XXIX] mutation is located in the anchor-probe binding site and not on the reporter-probe binding site (Fig. 1D). To examine the effect of mutations on the anchor probe, we genotyped a patient with a heterozygous [XXIX] mutation using primer/probe set G (Fig. 3F). We found no change in the melting curves between the wild-type allele and the [XXIX] allele, thereby suggesting that point mutations within the anchor probe sequence have little effect on the melting curve analysis.

3.2. Validation

The genotypes determined at Tohoku University using the proposed method and those determined at Kagoshima University using a previously published method were identical for the 11 common mutations (Table S1 in supplementary material). We performed a similar test using DNA samples purified from filter-paper blood samples to determine if this method could be used for newborn screening. The genotypes determined in both laboratories were identical for all 26 DNA samples (Table S2 in supplementary material).

3.3. Frequency of eleven prevalent mutations

We found four heterozygous carriers of mutation [I], three of mutation [II], and two of mutation [V]. In addition, primer/probe set G detected one heterozygous mutation, which was confirmed as mutation [VIII] by direct sequencing. Altogether, 10 mutations were detected in 420 Japanese healthy controls.

4. Discussion

We developed a simple and rapid genetic test using real-time PCR combined with the HybProbe system for the 11 prevalent mutations in *SLC25A13*: mutations [I], [II], [III], [IV], [V], [VI], [VII], [VIII], [IX], [XIX], and [XXI]. This genetic test is a closed-tube assay in which no post-PCR handling of the samples is required. In addition, the genotyping is completed within 1 h. This test can utilize DNA samples purified from both peripheral blood and filter-paper blood. The reliability of the test was confirmed by genotyping 76 blind DNA samples from patients with citrin deficiency, including 50 peripheral blood and 26 filter-paper blood DNA samples. Because screening for the 11 targeted mutations would identify 95% of mutant alleles in the Japanese population [19], both, one, and no mutant alleles are expected to be identified in 90.4%, 9.3%, and less than 0.3% of patients, respectively. This genetic test would be useful not only in Japan but also other East Asian countries, including China, Korea, Taiwan and Vietnam, in which the same mutations are prevalent. Our test is expected to detect 76–87% of the mutant alleles in the Chinese population [12,19,25], 95–100% in the Korean population [12,19,26], 60–68% in the Taiwanese population [27,28], and 100% in the Vietnamese population [12,19]. If we were to prepare a primer/probe set for mutation [X]:g.IVS6+5G>A [12], which is prevalent in Taiwan, the estimated sensitivity would exceed 90% in the Taiwanese population [27,28].

Recently, the high resolution melting (HRM) method was reported to be suitable for the screening of mutations in the diagnosis of citrin deficiency [28]. HRM analysis is a closed-tube assay that screens for any base changes in the amplicons. The presence of SNPs anywhere on the amplicons can affect the melting curve, thereby suggesting that HRM is not suitable for screening for known mutations, but rather, is best suited to screening for unknown mutations. When we detected one heterozygous prevalent mutation, we performed HRM screening for all 17 exons of *SLC25A13*. After HRM screening, only the HRM-positive exons were subjected to direct sequencing analysis. Several mutant alleles were identified using this approach.

The frequency of homozygotes, including compound heterozygotes, presenting *SLC25A13* mutations in the population at Kagoshima (a prefecture in the southern part of Japan) has been calculated to be 1/17,000 based on the carrier rate (1/65) [19]. The prevalence of NICCD has been also reported to be 1/17,000–34,000 [29]. In this study, the carrier rate in Miyagi (a prefecture in northern Japan) was 1/42 (95% confidential interval, 1/108–1/26), thereby yielding an estimated frequency of patients with citrin deficiency of 1/7,100. Our result, together with the previous report [19], suggests that a substantial fraction of the homozygotes or compound heterozygotes of SLC25A13 mutations was asymptomatic during the neonatal period.

The early and definitive diagnosis of citrin deficiency may be beneficial for patients with citrin deficiency by encouraging specific dietary habits and avoiding iatrogenic worsening of brain edema by glycerol infusion when patients develop encephalopathy [30,31]. Because the screening of blood citrulline levels by tandem mass analysis at birth does not detect all patients with citrin deficiency, the development of a genetic test would be welcomed. In this study, we demonstrated that genomic DNA extracted from filter paper blood samples was correctly genotyped, thereby indicating the feasibility of newborn screening using this genetic test. If 100,000 babies in the northern part of Japan were screened by this method, we would detect 14 homozygotes or compound heterozygotes with *SLC25A13* mutations and 2400 heterozygous carriers. In 2400 heterozygous carriers, we would expect to observe only 1 to 2 compound heterozygotes with one target and one non-target mutation. The estimated frequency of babies with two non-target mutations is 0.04/100,000. Our genetic method would therefore allow us to screen newborn babies efficiently. If we performed this genetic test in a high-throughput real-time PCR system, such as a 384- or 1,536-well format, the cost per sample could be lowered.

In conclusion, we have established a rapid and simple detection system using the HybProbe assay for the 11 prevalent mutations in *SLC25A13*. This system could be used to screen newborns for citrin deficiency and may facilitate the genetic diagnosis of citrin deficiency, especially in East Asian populations.

Supplementary materials related to this article can be found online at doi:10.1016/j.ymgme.2011.12.024.

Acknowledgments

The authors acknowledge the contribution of Dr. Keiko Kobayashi, who passed away on December 21th, 2010. Dr. Kobayashi discovered that the *SLC25A13* gene is responsible for citrin deficiency and devoted much of her life to elucidating the mechanism of citrin deficiency. This work was supported by grants from the Ministry of Education, Culture, Sports, Science, and Technology and the Ministry of Health, Labor, and Public Welfare.

References

[1] K. Kobayashi, D.S. Sinasac, M. Iijima, A.P. Boright, L. Begum, J.R. Lee, T. Yasuda, S. Ikeda, R. Hirano, H. Terazono, M.A. Crackower, I. Kondo, L.C. Tsui, S.W. Scherer, T. Saheki, The gene mutated in adult-onset type II citrullinaemia encodes a putative mitochondrial carrier protein, Nat. Genet. 22 (1999) 159–163.
[2] T. Ohura, K. Kobayashi, Y. Tazawa, I. Nishi, D. Abukawa, O. Sakamoto, K. Iinuma, T. Saheki, Neonatal presentation of adult-onset type II citrullinemia, Hum. Genet. 108 (2001) 87–90.
[3] Y. Tazawa, K. Kobayashi, T. Ohura, D. Abukawa, F. Nishinomiya, Y. Hosoda, M. Yamashita, I. Nagata, Y. Kono, T. Yasuda, N. Yamaguchi, T. Saheki, Infantile cholestatic jaundice associated with adult-onset type II citrullinemia, J. Pediatr. 138 (2001) 735–740.
[4] T. Tomomasa, K. Kobayashi, H. Kaneko, H. Shimura, T. Fukusato, M. Tabata, Y. Inoue, S. Ohwada, M. Kasahara, Y. Morishita, M. Kimura, T. Saheki, A. Morikawa, Possible clinical and histologic manifestations of adult-onset type II citrullinemia in early infancy, J. Pediatr. 138 (2001) 741–743.
[5] T. Shigeta, M. Kasahara, T. Kimura, A. Fukuda, K. Sasaki, K. Arai, A. Nakagawa, S. Nakagawa, K. Kobayashi, S. Soneda, H. Kitagawa, Liver transplantation for an

infant with neonatal intrahepatic cholestasis caused by citrin deficiency using heterozygote living donor, Pediatr. Transplant. 14 (2009) E86–88.
[6] M. Kasahara, S. Ohwada, T. Takeichi, H. Kaneko, T. Tomomasa, A. Morikawa, K. Yonemura, K. Asonuma, K. Tanaka, K. Kobayashi, T. Saheki, I. Takeyoshi, Y. Morishita, Living-related liver transplantation for type II citrullinemia using a graft from heterozygote donor, Transplantation 71 (2001) 157–159.
[7] Y. Takashima, M. Koide, H. Fukunaga, M. Iwai, M. Miura, R. Yoneda, T. Fukuda, K. Kobayashi, T. Saheki, Recovery from marked altered consciousness in a patient with adult-onset type II citrullinemia diagnosed by DNA analysis and treated with a living related partial liver transplantation, Intern. Med. 41 (2002) 555–560.
[8] A. Tamamori, Y. Okano, H. Ozaki, A. Fujimoto, M. Kajiwara, K. Fukuda, K. Kobayashi, T. Saheki, Y. Tagami, T. Yamano, Neonatal intrahepatic cholestasis caused by citrin deficiency: severe hepatic dysfunction in an infant requiring liver transplantation, Eur. J. Pediatr. 161 (2002) 609–613.
[9] T. Ohura, K. Kobayashi, Y. Tazawa, D. Abukawa, O. Sakamoto, S. Tsuchiya, T. Saheki, Clinical pictures of 75 patients with neonatal intrahepatic cholestasis caused by citrin deficiency (NICCD), J. Inherit. Metab. Dis. 30 (2007) 139–144.
[10] T. Yasuda, N. Yamaguchi, K. Kobayashi, I. Nishi, H. Horinouchi, M.A. Jalil, M.X. Li, M. Ushikai, M. Iijima, I. Kondo, T. Saheki, Identification of two novel mutations in the SLC25A13 gene and detection of seven mutations in 102 patients with adult-onset type II citrullinemia, Hum. Genet. 107 (2000) 537–545.
[11] N. Yamaguchi, K. Kobayashi, T. Yasuda, I. Nishi, M. Iijima, M. Nakagawa, M. Osame, I. Kondo, T. Saheki, Screening of SLC25A13 mutations in early and late onset patients with citrin deficiency and in the Japanese population: identification of two novel mutations and establishment of multiple DNA diagnosis methods for nine mutations, Hum. Mutat. 19 (2002) 122–130.
[12] Y.B. Lu, K. Kobayashi, M. Ushikai, A. Tabata, M. Iijima, M.X. Li, L. Lei, K. Kawabe, S. Taura, Y. Yang, T.-T. Liu, S.-H. Chiang, K.-J. Hsiao, Y.-L. Lau, L.-C. Tsui, D.H. Lee, T. Saheki, Frequency and distribution in East Asia of 12 mutations identified in the SLC25A13 gene of Japanese patients with citrin deficiency, J. Hum. Genet. 50 (2005) 338–346.
[13] E. Ben-Shalom, K. Kobayashi, A. Shaag, T. Yasuda, H.-Z. Gao, T. Saheki, C. Bachmann, O. Elpeleg, Infantile citrullinemia caused by citrin deficiency with increased dibasic amino acids, Mol. Genet. Metab. 77 (2002) 202–208.
[14] J. Takaya, K. Kobayashi, A. Ohashi, M. Ushikai, A. Tabata, S. Fujimoto, F. Yamato, T. Saheki, Y. Kobayashi, Variant clinical courses of 2 patients with neonatal intrahepatic cholestasis who have a novel mutation of SLC25A13, Metab. Clin. Exp. 54 (2005) 1615–1619.
[15] A. Luder, A. Tabata, M. Iijima, K. Kobayashi, H. Mandel, Citrullinaemia type 2 outside East Asia: Israeli experience, J. Inherit. Metab. Dis. 29 (2006) 59.
[16] T. Hutchin, M. Preece, K. Kobayashi, T. Saheki, R. Brown, D. Kelly, P. McKiernan, A. Green, U. Baumann, Neonatal intrahepatic cholestasis caused by citrin deficiency (NICCD) in a European patient, J. Inherit. Metab. Dis. 29 (2006) 112.
[17] J.-S. Sheng, M. Ushikai, M. Iijima, S. Packman, K. Weisiger, M. Martin, M. McCracken, T. Saheki, K. Kobayashi, Identification of a novel mutation in a Taiwanese patient with citrin deficiency, J. Inherit. Metab. Dis. 29 (2006) 163.
[18] J.M. Ko, G.-H. Kim, J.-H. Kim, J.Y. Kim, J.-H. Choi, M. Ushikai, T. Saheki, K. Kobayashi, H.-W. Yoo, Six cases of citrin deficiency in Korea, Int. J. Mol. Med. 20 (2007) 809–815.
[19] A. Tabata, J.-S. Sheng, M. Ushikai, Y.-Z. Song, H.-Z. Gao, Y.-B. Lu, F. Okumura, M. Iijima, K. Mutoh, S. Kishida, T. Saheki, K. Kobayashi, Identification of 13 novel mutations including a retrotransposal insertion in SLC25A13 gene and frequency of 30 mutations found in patients with citrin deficiency, J. Hum. Genet. 53 (2008) 534–545.
[20] P.S. Bernard, R.S. Ajioka, J.P. Kushner, C.T. Wittwer, Homogeneous multiplex genotyping of hemochromatosis mutations with fluorescent hybridization probes, Am. J. Pathol. 153 (1998) 1055–1061.
[21] C.N. Gundry, P.S. Bernard, M.G. Herrmann, G.H. Reed, C.T. Wittwer, Rapid F508del and F508C assay using fluorescent hybridization probes, Genet. Test. 3 (1999) 365–370.
[22] T. Saheki, K. Kobayashi, I. Inoue, Hereditary disorders of the urea cycle in man: biochemical and molecular approaches, Rev. Physiol. Biochem. Pharmacol. 108 (1987) 21–68.
[23] K. Kobayashi, M. Horiuchi, T. Saheki, Pancreatic secretory trypsin inhibitor as a diagnostic marker for adult-onset type II citrullinemia, Hepatology 25 (1997) 1160–1165.
[24] Y. Tazawa, K. Kobayashi, D. Abukawa, I. Nagata, S. Maisawa, R. Sumazaki, T. Iizuka, Y. Hosoda, M. Okamoto, J. Murakami, S. Kaji, A. Tabata, Y.B. Lu, O. Sakamoto, A. Matsui, S. Kanzaki, G. Takada, T. Saheki, K. Iinuma, T. Ohura, Clinical heterogeneity of neonatal intrahepatic cholestasis caused by citrin deficiency: case reports from 16 patients, Mol. Genet. Metab. 83 (2004) 213–219.
[25] H.Y. Fu, S.R. Zhang, X.H. Wang, T. Saheki, K. Kobayashi, J.S. Wang, The mutation spectrum of the SLC25A13 gene in Chinese infants with intrahepatic cholestasis and aminoacidemia, J. Gastroenterol. 46 (2011) 510–518.
[26] K. Kobayashi, Y.B. Lu, M.X. Li, I. Nishi, K.-J. Hsiao, K. Choeh, Y. Yang, W.-L. Hwu, J.K.V. Reichardt, F. Palmieri, Y. Okano, T. Saheki, Screening of nine SLC25A13 mutations: their frequency in patients with citrin deficiency and high carrier rates in Asian populations, Mol. Genet. Metab. 80 (2003) 356–359.
[27] T. Saheki, K. Kobayashi, M. Iijima, M. Horiuchi, L. Begum, M.A. Jalil, M.X. Li, Y.B. Lu, M. Ushikai, A. Tabata, M. Moriyama, K.-J. Hsiao, Y. Yang, Adult-onset type II citrullinemia and idiopathic neonatal hepatitis caused by citrin deficiency: involvement of the aspartate glutamate carrier for urea synthesis and maintenance of the urea cycle, Mol. Genet. Metab. 81 (Suppl 1) (2004) S20–S26.
[28] J.T. Lin, K.J. Hsiao, C.Y. Chen, C.C. Wu, S.J. Lin, Y.Y. Chou, S.C. Shiesh, High resolution melting analysis for the detection of SLC25A13 gene mutations in Taiwan, Clin. Chim. Acta 412 (2011) 460–465.
[29] Y. Shigematsu, S. Hirano, I. Hata, Y. Tanaka, M. Sudo, N. Sakura, T. Tajima, S. Yamaguchi, Newborn mass screening and selective screening using electrospray tandem mass spectrometry in Japan, J. Chromatogr. B Analyt. Technol. Biomed. Life Sci. 776 (2002) 39–48.
[30] M. Yazaki, Y.-i. Takei, K. Kobayashi, T. Saheki, S.-I. Ikeda, Risk of worsened encephalopathy after intravenous glycerol therapy in patients with adult-onset type II citrullinemia (CTLN2), Intern. Med. 44 (2005) 188–195.
[31] H. Takahashi, T. Kagawa, K. Kobayashi, H. Hirabayashi, M. Yui, L. Begum, T. Mine, S. Takagi, T. Saheki, Y. Shinohara, A case of adult-onset type II citrullinemia—deterioration of clinical course after infusion of hyperosmotic and high sugar solutions, Med. Sci. Monit. 12 (2006) CS13–CS15.

OPEN ACCESS Freely available online PLoS one

Development of a Multi-Step Leukemogenesis Model of MLL-Rearranged Leukemia Using Humanized Mice

Kunihiko Moriya[1,2], Makiko Suzuki[1], Yohei Watanabe[2], Takeshi Takahashi[1,4], Yoko Aoki[3], Toru Uchiyama[2], Satoru Kumaki[2], Yoji Sasahara[2], Masayoshi Minegishi[5], Shigeo Kure[2], Shigeru Tsuchiya[2], Kazuo Sugamura[1,6], Naoto Ishii[1]*

1 Department of Microbiology and Immunology, Tohoku University Graduate School of Medicine, Sendai, Japan, **2** Department of Pediatrics, Tohoku University Graduate School of Medicine, Sendai, Japan, **3** Department of Medical Genetics, Tohoku University Graduate School of Medicine, Sendai, Japan, **4** Central Institute for Experimental Animals, Kawasaki, Japan, **5** Division of Blood Transfusion, Tohoku University Hospital, Sendai, Japan, **6** Miyagi Cancer Center, Natori, Japan

Abstract

Mixed-lineage-leukemia (MLL) fusion oncogenes are intimately involved in acute leukemia and secondary therapy-related acute leukemia. To understand MLL-rearranged leukemia, several murine models for this disease have been established. However, the mouse leukemia derived from mouse hematopoietic stem cells (HSCs) may not be fully comparable with human leukemia. Here we developed a humanized mouse model for human leukemia by transplanting human cord blood-derived HSCs transduced with an MLL-AF10 oncogene into a supra-immunodeficient mouse strain, NOD/Shi-*scid*, IL-2Rγ$^{-/-}$ (NOG) mice. Injection of the MLL-AF10-transduced HSCs into the liver of NOG mice enhanced multilineage hematopoiesis, but did not induce leukemia. Because active mutations in ras genes are often found in MLL-related leukemia, we next transduced the gene for a constitutively active form of K-ras along with the MLL-AF10 oncogene. Eight weeks after transplantation, all the recipient mice had developed acute monoblastic leukemia (the M5 phenotype in French-American-British classification). We thus successfully established a human MLL-rearranged leukemia that was derived *in vivo* from human HSCs. In addition, since the enforced expression of the mutant K-ras alone was insufficient to induce leukemia, the present model may also be a useful experimental platform for the multi-step leukemogenesis model of human leukemia.

Citation: Moriya K, Suzuki M, Watanabe Y, Takahashi T, Aoki Y, et al. (2012) Development of a Multi-Step Leukemogenesis Model of MLL-Rearranged Leukemia Using Humanized Mice. PLoS ONE 7(6): e37892. doi:10.1371/journal.pone.0037892

Editor: Kevin D. Bunting, Emory University, United States of America

Received February 24, 2012; **Accepted** April 30, 2012; **Published** June 20, 2012

Funding: This work was supported in part by a grant-in-aid (#11102000101000410O) for scientific research from the Japan Society and Technology Agency, by a grant from Japan Science and Technology Agency, and by a grant from Kato Memorial Bioscience Foundation. The funders had no role in study design, data collection and analysis, decision to publish, or preparation of the manuscript. No additional external funding was received for this study.

Competing Interests: The authors have declared that no competing interests exist.

* E-mail: ishiin@med.tohoku.ac.jp

Introduction

Chromosomal translocations that result in MLL (mixed-lineage leukemia)-fusion oncogenes are associated with acute myeloid leukemia (AML), acute lymphoblastic leukemia (ALL), myelodysplastic syndrome, and secondary therapy-related acute leukemia [1]. More than 60 partner genes that form MLL-fusion oncogenes have been identified [2], and the partner usually characterizes the specific pathological phenotype of the MLL-rearranged leukemia. For example, MLL-rearranged AMLs, more than 60% of which involve the MLL-AF9, MLL-AF10, or MLL-AF6 fusion gene, often exhibit the morphological subtypes acute myelomonoblastic leukemia and monoblastic leukemia, which are classified as French-American-British (FAB) M4 and M5, respectively [3]. Although patients with MLL-rearranged leukemia usually show a poor prognosis and are sometimes resistant to therapy [3,4], the development of efficient therapies targeting the MLL-fusion genes has been slow, in part because much is still unknown about the cellular and molecular mechanisms underlying this disease.

To gain insight into the etiology and pathogenesis of MLL-rearranged leukemia, several mouse models have been developed. Mice with a knocked-in MLL-AF9 fusion gene develop AML as they age [5], although in humans the congenital MLL-AF9 rearrange typically affects infants. Leukemia has also been generated in mice by exogenously expressing an MLL-fusion gene in the animals or by transplanting mouse hematopoietic stem cells (HSCs) that have been retrovirally transduced with an MLL-fusion gene [6]. However, the phenotype and pathogenesis of the leukemia produced in these murine models sometimes do not match those observed in human leukemia associated with the same genetic lesion. For example, the MLL-ENL fusion gene is frequently associated with B-precursor ALL in humans, but generates AML in mice [7]. Thus, there is a gap in our understanding about mouse versus human leukemogenesis, and further leukemia modeling studies using human primary leukemia cells are needed [8].

In vivo studies in which primary human leukemia cells were transplanted into immunodeficient mice, provided significant advances in our understanding of the pathogenesis of human leukemia [9,10]. However, these models, in which the leukemia cells had already developed in human patients before being transplanted into mice, are not suitable for studying physiological leukemogenesis, including the initiation and progression processes since these processes do not occur in the model. Therefore, a new experimental model for analyzing leukemogenesis in which

primary human HSCs are converted into leukemia cells by genetic hits is needed.

In the past two decades, a number of studies have tried to graft human HSCs into immunodeficient mice, but these attempts to reconstitute human blood cells in mice have failed [11]. However, the recent development of a new immunodeficient mouse strain has opened up the possibility for generating better xenotransplantation systems. NOD/SCID mice with a targeted mutation of the IL-2-receptor γ chain gene (NOD/Shi-*scid* IL-2Rγ$^{-/-}$ (NOG) and NOD/LtSz-scid IL-2Rγ$^{-/-}$ (NSG) mice) lack T, B, and NK cells and some innate immunity functions [11,12]. When human HSCs are transplanted into these mice, human T, B, NK, and dendritic cells develop normally and are maintained in the mice for at least 10 months[13–17]. Thus, these immunodeficient mice may be good recipients for examining, not only the normal development of human HSCs, but also their abnormal development, including leukemogenesis. Two previous studies modeled the initiation and progression of human acute leukemia by ectopically expressing MLL-fusion genes in human HSCs, and transplanting these cells into special immunodeficient mice [18,19]. Dick et al demonstrated that ectopic expression of AF9 or MLL-ENL in human HSCs caused leukemia in NOD/SCID mice in which the NK cells were depleted by an anti-NK cell antibody [18]. Similarly, Mulloy et al successfully modeled acute leukemia by transducing MLL-AF9 into human HSCs, and transplanting these cells into NOD/SCID mice that expressed transgenic human SCF, GM-CSF, and IL-3 genes [19]. However, in a similar model using NSG mice, the enforced expression of MLL-AF4 in HSCs did not induce leukemia [20].

Despite intensive studies on MLL-ENL, MLL-AF4, and MLL-AF9, there has been no report investigating the *in vivo* oncogenic potential of MLL-AF10 in human HSCs, even though MLL-AF10 is the second most common MLL rearrangement (13%) in pediatric MLL-rearranged AML [3]. Here, using NOG mice, we demonstrated that MLL-AF10 could enhance the multilineage hematopoiesis of human HSCs, even though the MLL-AF10 in mouse HSCs preferentially enhances myeloid differentiation [21,22]. More importantly, the co-transfection of MLL-AF10 with an active form of the K-ras gene induced acute monoblastic leukemia with the FAB M5 phenotype. These results provide a novel leukemia model using human cells showing the requirement of two genetic hits for leukemogenesis.

Methods

All procedures were performed according to the protocols approved by the Institutional Committee for Use and Care of Laboratory Animals of Tohoku University, which was granted by Tohoku University Ethics Review Board (No. 2010MA165) and the Guide for Care and Use of Laboratory Animals published by the U.S. National Institutes of Health (NIH publication 85-23, revised 1996).

CD34$^+$ Hematopoietic Stem Cell Isolation

Cord blood from full-term human deliveries was obtained from the Miyagi Cord Blood Bank (Miyagi, Japan) and RIKEN Bioresource Center Cell Bank (Tsukuba, Japan), following the institutional guidelines approved by the Tohoku University Committee on Clinical Investigations. Mononuclear cells were isolated from the cord blood by density gradient centrifugation using Lymphocyte Separation Medium (MP Biomedicals, Solon, OH, USA) after removing the phagocytes with silica (Immuno Biological Laboratories, Takasaki, Japan). The cells were washed and suspended in PBS containing 2%FCS. CD34$^+$ stem cells were obtained by magnetic cell sorting (MACS) (Miltenyi Biotech, Bergisch Gladbach, Germany). Briefly, CD34$^+$ cells were labeled with a biotin-conjugated anti-human CD34 monoclonal antibody (Serotec, Oxford, UK) after blocking the Fc receptor. The cells were then incubated with anti-biotin Microbeads (Miltenyi Biotech). The magnetically labeled CD34$^+$ cells were purified twice on LS columns (Miltenyi Biotech). The purity of the CD34$^+$ fraction was >95%. The purified CD34$^+$ cells were suspended in Cell Banker (Juji Field, Tokyo, Japan) and cryopreserved at −80°C in a deep freezer until use.

Plasmid Construction

The retroviral vector, pDΔNsam-IRES-EGFP, which is based on Murine Stem Cell Virus with enhanced green fluorescent protein (EGFP) as a marker under an internal ribosomal entry site (IRES), was kindly provided by Dr. Masafumi Onodera (Tsukuba University) [23]. PLAT-F, a package cell line that produces a pseudotype virus with an RD114 envelope, was previously established and provided by Dr. Toshio Kitamura (Institute of Medical Science, University of Tokyo) [24]. The human MLL-AF10 cDNA [22], which was kindly provided by Dr. M.L. Cleary (Stanford University), was inserted into a cloning site in the pDΔNsam-IRES-EGFP vector to make the pDΔNsam-MLL-AF10 plasmid. To construct the pDΔNsamIRES VENUS vector, the EGFP cDNA of the retroviral vector was replaced with Venus cDNA [25], which was provided by Dr. Hiroyuki Miyoshi (RIKEN, Tsukuba). The human flag-tagged K-ras^{G12V} cDNA, which was previously described [26], was inserted into the Xho I site in the cloning site of pDΔNsamIRES Venus to make pDΔNsam-K-ras^{G12V}.

Gene Delivery into CD34$^+$ Cells by Retrovirus

The CD34$^+$ cells isolated from cord blood were cultured in X-VIVO15 (Cambrex Bioscience, Walkersville, MD, USA), supplemented with 1% human serum albumin (HSA) (Kaketsuken, Kumamoto, Japan) and stimulated with a cytokine cocktail [100 ng/ml stem cell factor, 100 ng/ml Flt-3 ligand, 100 ng/ml thrombopoietin, and 100 ng/ml IL-6 (Peprotech)] in a 24-well plate (2×10^5 per well) for 48 h. The stimulated CD34$^+$ cells were then harvested and placed into non-tissue culture-treated 6-well plates (Becton Dickinson) that had been coated with 20 μg/ml CH-296, a recombinant fibronectin fragment (Retronectin, Takara, Japan). (3×10^5 cells per well) in the presence of the respective virus supernatant. The virus supernatants were diluted 1:2 with X-VIVO15 containing 1% HSA and the cytokine cocktail described above. Every 12 h, the medium was replaced with fresh virus supernatant. After 48 h of culture, the frequency of GFP- and/or Venus-expressing CD34$^+$ cells was examined by FACS.

Cell Transplantation into Mice

NOD/Shi-*scid*, IL-2Rγ$^{-/-}$ (NOG) mice were obtained from the Central Institute for Experimental Animals (CIEA, Kawasaki, Japan) and maintained in an animal facility at Tohoku University Graduate School of Medicine under specific pathogen free conditions. All procedures were performed according to the protocols approved by Tohoku University Ethics Review Board (No. 2010MA165). Neonatal (1–3 days) NOG mice were irradiated with 30 cGy of X-rays, and the cultured CD34$^+$ cells ($1.0-1.5\times10^5$) in 70 μl PBS were intrahepatically injected into the mice later the same day. From one cord blood sample, donor cells could be prepared for transplantation into 3 recipient mice. Therefore, 2 to 4 different cord blood samples were used for each mouse group. Since even NOG mouse sometimes failed to engraft human HSCs, 9 recipient mice that had no human CD45$^+$

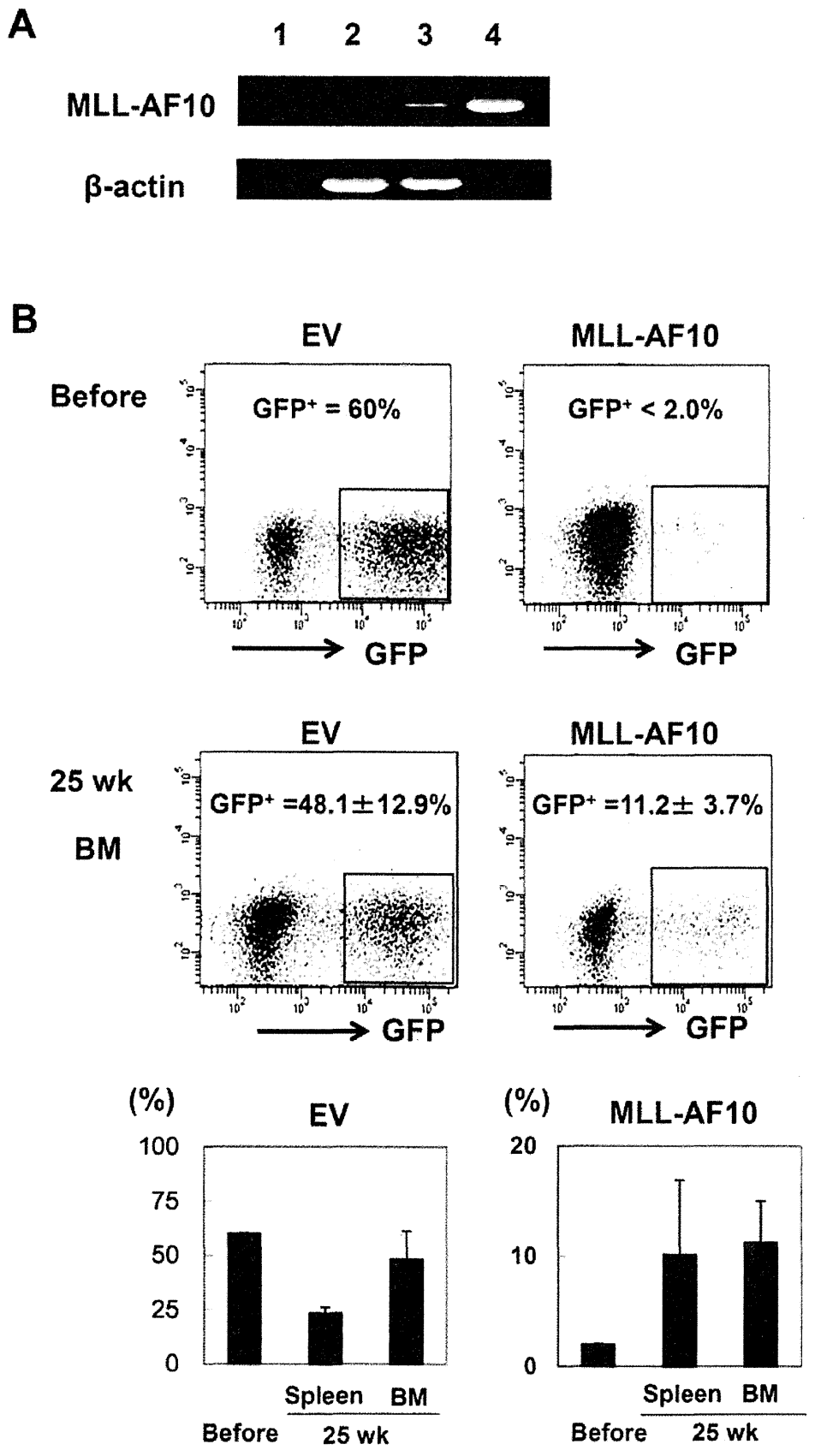
A
1
2
3
4
MLL-AF10
β-actin
B
EV
MLL-AF10
Before
GFP+ = 60%
GFP+ < 2.0%
GFP
GFP
25 wk
BM
GFP+ =48.1±12.9%
GFP+ =11.2± 3.7%
GFP
GFP
(%)
EV
100
75
50
25
0
Spleen
BM
Before
25 wk
(%)
MLL-AF10
20
10
0
Spleen
BM
Before
25 wk

Figure 1. Enforced expression of MLL-AF10 augmented multilineage hematopoiesis, but was insufficient to induce leukemogenesis in vivo. (A) Representative RT-PCR results confirming the long-term expression of the MLL-AF10 transcript in the BM cells of mice 25 weeks after transplantation (lane 1; water, lane 2; cells from a mouse in the EV-transfused group, lane 3; cells from a mouse in the MLL-AF10-transfused group, and lane 4; positive control (MLL-AF10 plasmid)). (B) Flowcytometric analysis of the frequency of GFP^+ cells. The indicated vector (EV, left or MLL-AF10, right)-transduced human $CD34^+$ cells, whose *in vitro* GFP expression is shown in the upper panels (Before) of the flowcytometric analysis, were transplanted into NOG mice. Twenty-five weeks later, the GFP-expressing cells gated on human $CD45^+$ hematopoietic cells in the BM was measured (lower panels of the FACS profiles). The data shown are representative of 3 independent experiments. The graphs show the frequency of GFP^+ cells in human $CD34^+$ cells just before transplantation (Before) and the mean ± SD of the frequency of GFP^- cells in the BM and spleen of mice receiving transplants of EV-transduced HSCs (n = 8) or of MLL-AF10-transduced HSCs (n = 6) 25 weeks after transplantation, in one representative experiment of three. Similar results were obtained in the 3 independent experiments.
doi:10.1371/journal.pone.0037892.g001

hematopoietic cell in the BM and spleen at the sacrifice were excluded from this study.

Antibodies and Flow Cytometric Analysis

Surface markers were detected with the following fluorescent human specific antibodies from BD Biosciences, San Jose, CA, USA: CD33-PE, HLA-DR-PE, CD14-PE, CD19-APC, CD11b-APC, CD15-APC, and CD45-APC-Cy7. To monitor the reconstitution of human blood in NOG mice, peripheral blood was periodically taken from the tail vein. To examine the spleen, bone marrow (BM), and liver, single-cell suspensions were prepared from the spleen and liver by mincing with metal mesh and from the BM by flushing the tibiae and femurs with PBS containing 2% FCS, using a 27-gauge needle. The cells were stained with the relevant antibodies for 15 min on ice, then washed with cold PBS containing 2% FCS, and stained with the appropriate secondary antibodies when necessary. After the final wash, the cells were subjected to flowcytometric analysis with a FACSCanto II cytometer (BD Biosciences). To distinguish between the EGFP (510 nm) and Venus (535 nm) fluorescences, an apporopiate combination of mirrors and optical filters was used. The proportion of each lineage was calculated using FACS Diva software (BD Biosciences).

Reverse Transcription-PCR (RT-PCR)

Total RNA was prepared from cells using Trizol Reagent (Invitrogen, Carlsbad, CA, USA). The concentration of total RNA was measured by a NanoDrop 1000 (Nanodrop Technologies Inc., Wilmington, DE, USA), and first-strand cDNA was synthesized using Superscript II (Invitrogen) with an oligo (dT) primer. The cDNA for MLL-AF10, Flag-K-ras, or β-actin was amplified with specific primers using Ex-Taq polymerase (Takara). The primer sets were as follows; MLL-AF10: forward, 5- ccaaaagaaaaggaaaaacca and reverse, 5-gacttcagcattcctaaaatgtca; Flag-K-ras: forward, 5-gactacaaagacgatgacg and reverse, 5-ccctgtcttgtctttgc; β-actin: forward, 5-gctcgtcgtcgacaacggctc and reverse, 5-caaacatgatctgggtcatcttctc.

DNA Extraction and Southern Blot Analysis

Genomic DNA was extracted from spleens using the GenElute™ Mammalian Genomic DNA Miniprep kit (Sigma-Aldrich, USA). For Southern blot analyses, 10 μg genomic DNA was digested with BglII (Toyobo, Osaka, Japan) overnight at 37°C and separated by electrophoresis on a 0.7% agarose gel for 12 h at 40 V. The DNA was transferred overnight to a Hybond N^+ membrane (GE Healthcare, Chalfont St. Giles, UK). The DNA was fixed onto the membrane with a UV Stratalinker 1800 (Stratagene). The membrane was probed with 10^6 cpm/ml of [$C^{32}P$]dCTP (Perkin Elmer)-labeled EGFP cDNA. This EGFP probe was derived from a 700-bp ScaI fragment of the pDANsam-IRES-EGFP vector, and radiolabeled using a random prime labeling kit (Takara). The membrane was then washed and exposed to a BAS-III imaging plate (Fuji Photo Film Co., LTD, Japan), and the image was produced and analyzed using a BAS-III software (Fuji Photo Film Co., LTD).

Histopathology

The BM, spleen, and liver were examined macroscopically, and the spleen was weighed. Tissues were fixed in 10% formalin for at least 48 hours. Hematoxylin and eosin staining or May-Giemsa staining was performed on 3-μm sections using a routine protocol. For CD45 immunostaining, after dewaxing and antigen retrieval by microwave, the sections were incubated for 1 h with mouse anti-human CD45 (Dako Japan, Tokyo). Immunodetection was performed using HRP as the visualization enzyme and DAB as the substrate chromogen. All slides were examined by light microscopy using an Olympus IX50 microscope (Olympus, Tokyo, Japan) and a SPOT camera.

Statistical Analysis

Data are presented as the mean ± standard deviation (SD). Statistical analyses were performed using either a paired or unpaired Student's t-test. Statistical significance was defined as a P-value <0.01 (**).

Results

Enforced Expression of MLL-AF10 Augmented Multilineage Hematopoiesis, but was Insufficient for Leukemogenesis in vivo

To examine the pathogenesis of the MLL-AF10 fusion gene during the differentiation of human blood cells from HSCs, MLL-AF10-infected cord blood $CD34^+$ cells were transplanted intrahepatically into sublethally irradiated neonatal NOG mice. None of the recipient mice showed any sign of disease, such as body weight loss or the appearance of abnormal peripheral leukocytes, 25 weeks after transplantation (data not shown). The expression of the transduced MLL-AF10 gene in the reconstituted human blood cells was confirmed (Figure 1A), indicating that the enforced expression of MLL-AF10 in human HSCs could not induce any hematological disorders including leukemia in this model. However, the MLL-AF10 appeared to augment hematopoiesis. As shown in Figure 1B, when empty control vector (EV) was transdused into human $CD34^+$ HSCs, the frequency of the GFP^+ population did not change significantly (60% before transplantation and 24% and 48% after transplantation in the spleen and BM, respectively) (Figure 1B). In contrast, when MLL-AF10 was exogenously expressed, the GFP^+ population markedly increased from 2% (before) to 11% (25 weeks after transplantation) (Figure 1B). Therefore, the MLL-AF10-positive blood cells may have a growth advantage *in vivo* compared to the MLL-AF10-negative normal blood cells ($CD45^+GFP^-$ cells).

We next characterized the lineage composition of the human $CD45^+GFP^+$ cells in the BM and spleen of both groups. The GFP^+ MLL-AF10-expressing cells did not show a skewed lineage differentiation compared to the EV-transfected hematopoietic

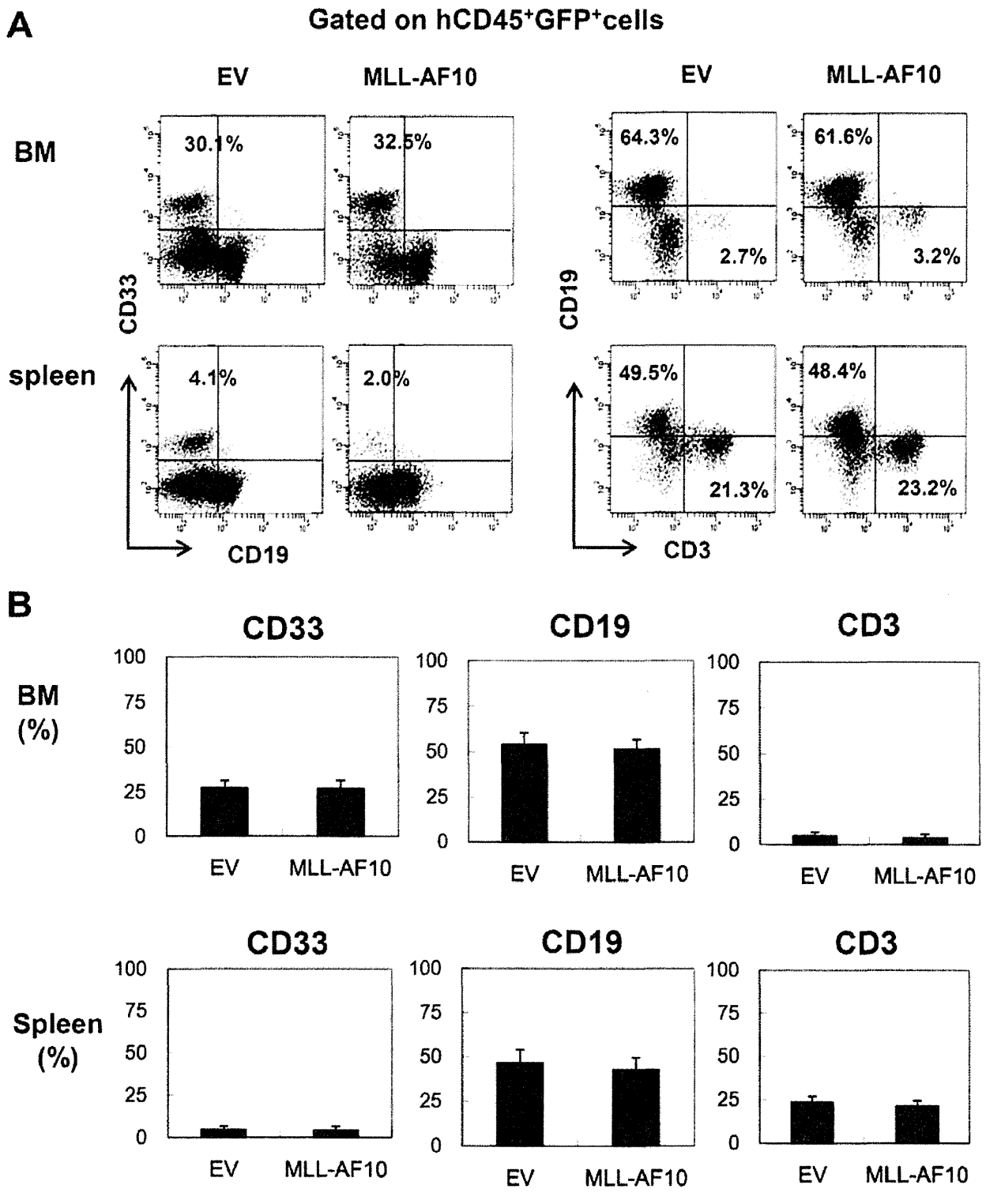

Figure 2. Flowcytometric analysis confirming multilineage engraftment. (A) Representative flowcytometric results of EV- or MLL-AF10-transduced human hematopoietic cells. The human CD45$^+$ GFP$^+$ cells were analyzed for their lineage distributions to B cells (CD19$^+$), T cells (CD3$^+$), and myeloid cells (CD33$^+$). (B) Multilineage differentiation of MLL-AF10-transduced cells. The data shows cells gated on the CD45$^+$GFP$^+$ cell population. The graph represents the mean ± SD of the frequencies of CD33$^+$ myeloid cells, CD19$^+$ B cells, and CD3$^+$ T cells in the BM (upper) and spleens (lower) of mice engrafted with EV-transduced (n = 8) or MLL-AF10-transduced (n = 6) CD34$^+$ HSCs. No difference in the graft composition between the EV- and MLL-AF10-expressing CD34$^+$ HSCs was found. Similar results were obtained in 3 independent experiments.
doi:10.1371/journal.pone.0037892.g002

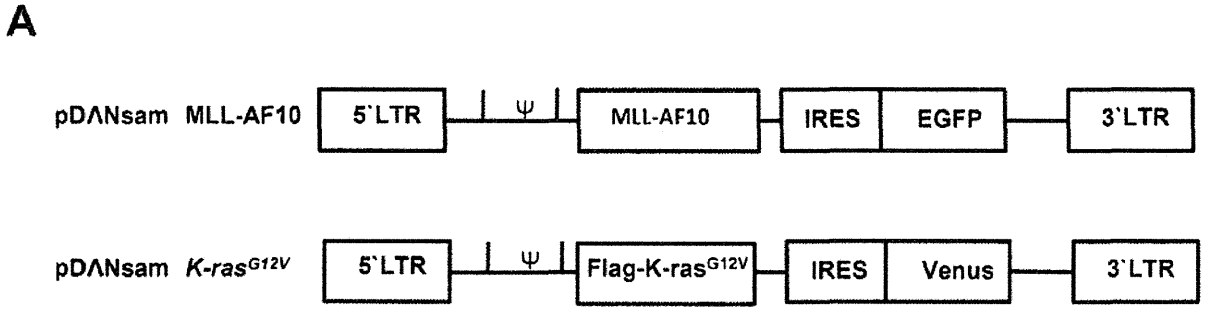

B

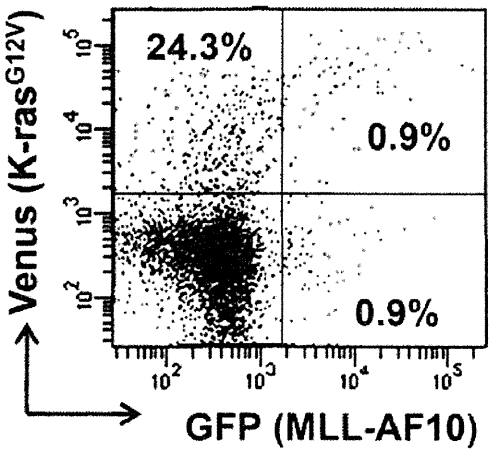

Summary of transplantation

	Efficiency	Cell No. ($\times 10^3$)
GFP+Venus+	0.8 - 0.9 %	1.0
GFP+Venus-	0.8 - 0.9 %	1.0
GFP-Venus+	22 - 24 %	31-33
GFP-Venus-	74- 76 %	97-115
Total	100%	130 -150

Figure 3. Co-transduction of activated K-ras and MLL-AF10 into CD34$^+$HSCs. (A) Schematic structure of the MLL-AF10-GFP and Flag-K-ras^{G12V}-Venus vectors. (B) Infectious efficiency of the MLL-AF10-GFP and Flag-K-ras^{G12V}-Venus co-transfection. The data and the summary shown in the flowcytometric analysis is representative of the transduced CD34$^+$ HSCs in 2 experiments.
doi:10.1371/journal.pone.0037892.g003

cells (Figures 2A and 2B). In contrast to the previous reports with mouse HSCs, which showed skewed myeloid differentiation by the exogenous expression of MLL-AF10 [21,22], the enforced expression of MLL-AF10 in human HSCs enhanced the hematopoietic repopulation of HSCs without affecting cell differentiation.

Co-transduction of Activated K-ras and MLL-AF10 into CD34$^+$ HSCs

As described above, transduction of the MLL-AF10 gene alone was not sufficient to induce leukemogenesis from human HSCs in the present model. Similarly, Menendez et al recently demonstrated that the MLL-AF4 gene alone cannot induce leukemia from human CD34$^+$ HSCs in a humanized mouse model [20]. These observations prompted us to generate a two-hit model of leukemogenesis using MLL-AF10 and one additional oncogene. We thus used the K-ras^{G12V} oncogene because K-ras^{G12V} is a very well-characterized oncogene, and because ras mutations are found in about 30% of the cases of pediatric MLL-rearranged AML [3]. To evaluate two hits in one cell, we needed to distinguish the MLL-AF10 and K-ras^{G12V} expressions. We thus retrovirally transfected CD34$^+$ HSCs with MLL-AF10-EGFP and K-ras^{G12V} that was co-expressed with the Venus fluorescent protein, which can be distinguished from EGFP by flowcytometry (Figure 3A). The MLL-AF10 and K-ras co-infected (GFP$^+$Venus$^+$) cells were quite rare (0.9%) (Figure 3B). Nevertheless, we injected the CD34$^+$ HSCs, which contained 74% non-transduced, 0.9% MLL-AF10-alone-transduced, 24% K-ras^{G12V}-alone-transduced, and 0.9% co-transduced cells, intrahepatically into NOG mice (Figure 3B).

Cooperation of MLL-AF10 with Activated K-ras Induced Acute Monoblastic Leukemia

By 8 weeks after transplantation, several mice in the MLL-AF10/K-ras^{G12V} co-transduced group showed a rough coat, slow movement, and weight loss, while no mice in the other groups (EV, MLL-AF10 alone, and K-ras^{G12V} alone) demonstrated any disease manifestations (data not shown). As the mice in the co-transduced group got sick, most of their peripheral leukocytes became double positive for GFP and Venus (Figure 4B). In addition, morphologically identifiable leukemia cells, characterized by abnormal nuclei and cytoplasmic vacuoles, were found in the peripheral blood (Figure 4C). The morphology of the leukemia cells was compatible with that of the M5 type of FAB classification, which is relatively common in MLL-rearranged AML. Furthermore, splenomegaly in the mice engrafted with the MLL-AF10/K-ras^{G12V} co-transduced human HSCs was observed 8 weeks after

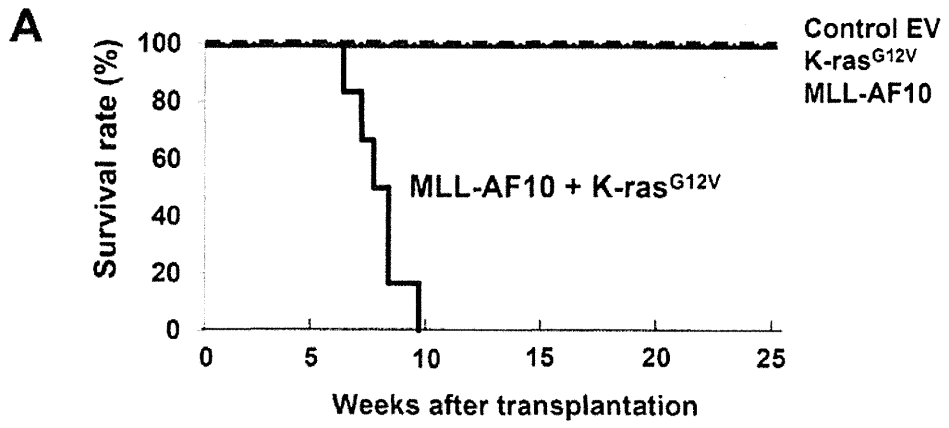
A
Survival rate (%)
100
80
60
40
20
0
0
5
10
15
20
25
Weeks after transplantation
MLL-AF10 + K-ras^{G12V}
Control EV
K-ras^{G12V}
MLL-AF10

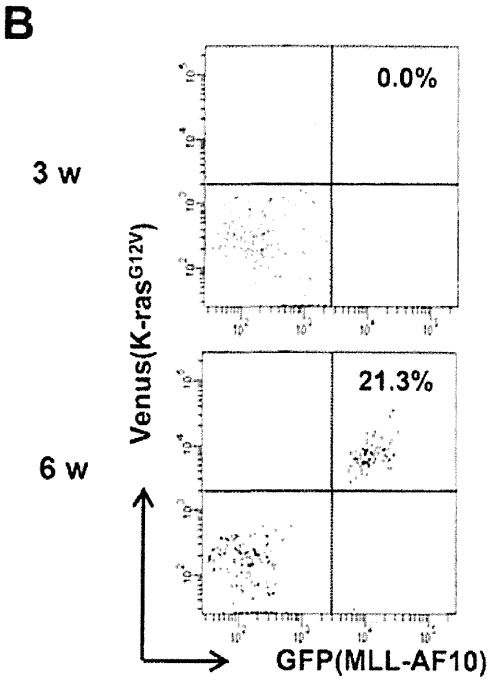
B
3 w
6 w
0.0%
21.3%
Venus(K-ras^{G12V})
GFP(MLL-AF10)

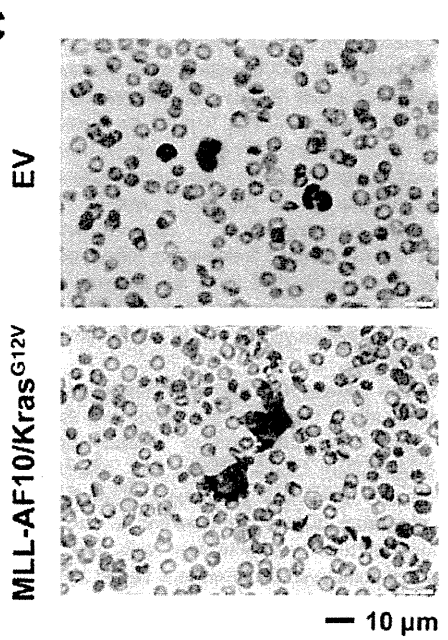
C
EV
MLL-AF10/Kras^{G12V}
10 μm

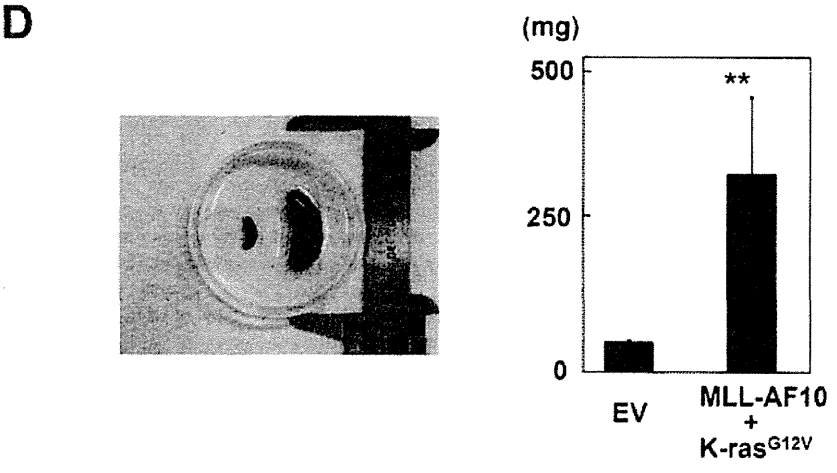
D
(mg)
500
250
0
**
EV
MLL-AF10
+
K-ras^{G12V}